The Bolting of Magnesium Components in Car Engines

Sarennah J.P. Longworth
Newnham College

A dissertation submitted for the degree of Master of Philosophy
to the University of Cambridge.

31st August 2001

Declaration

This dissertation is the result of my own work and does not include any work that is the outcome of collaboration. No part of this dissertation has been submitted at Cambridge or any other University for a degree, diploma or other qualification. The total length of this dissertation is 13150 words.

Sarennah J.P. Longworth
Cambridge
31st August 2001

Acknowledgements

The author would like to thank the following: Professor Bhadeshia for his continual enthusiasm, support and cheerfulness and particularly for his comments on the first version of this report; Thomas Hermansson and Ingemar Bertilsson for providing the data; Ingemar Bertilsson for sending me numerous papers; Thomas Sourmail for providing the Models Manager software and providing technical assistance with the hardware and software; and to Oomps and Kerry for their help with the proof reading.

Model 1 and Model 3 have been submitted to the Materials Algorithm Project for dissemination: http://www.msm.cam.ac.uk/map.

This project is dedicated to Polly for her constant cheerful presence.

Abstract

The automotive industry is striving to produce lighter vehicles. At present this is achieved through the use of ultralight steels, aluminium alloys and magnesium alloys for some body parts. Magnesium has the highest strength-to-weight ratio of any structural metal and so engineers are keen to use as much magnesium as possible in their vehicles. However, magnesium alloys creep, even at room temperature, restricting their use.

This project focuses on the problem of bolting together magnesium alloys components at temperatures around 100^{o}C, such as those found in car engines. The bolted joints undergo stress relaxation even at such low temperatures. The problem of stress relaxation in magnesium alloy AZ91D is investigated using four physical and non-physical neural network models. These models have half the noise level of the experimental results used to make the networks and their predictive qualities are shown to be an improvement over standard empirical models. The networks were used to attempt to reproduce published results and to calculate the activation energy for self-diffusion in magnesium.

Contents

1 Introduction

The weight of the average family car has increased by 20% over the last 20 years (Fig. 1). Most of the increased weight is a result of increased average engine size and the addition of safety features such as crumple zones and roll cages.

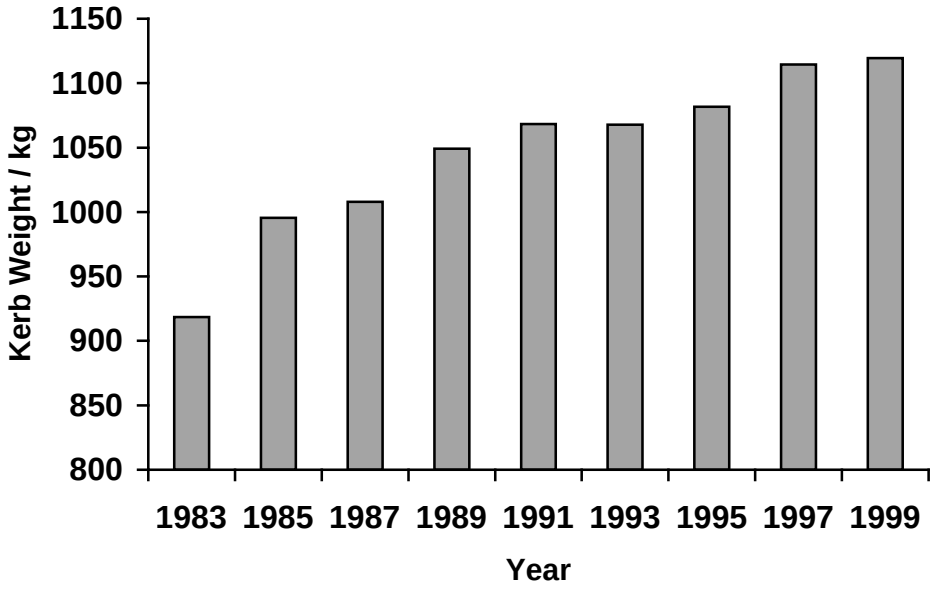

Fig 1
The kerb weight[1] of the four door hatchback Ford Fiesta from 1983 to 1999 [2].

Customers' awareness of fuel efficiency has been made more acute by increasing fuel prices and the popularity of environmental issues. Car manufacturers are also affected by legislation to control air quality, such as the European Union directive that cars should produce less than 120 g of CO_2 per kilometre by 2005 [3], and are approaching this problem by attempting to reduce the weight of their cars. "Concept cars" produced in recent years have been lightweight, for example, the Ford P2000 which weighs only 544.3 kg [4]. The weight reductions have been made possible by the replacement of steel by light metal alloys, usually aluminium or magnesium. In production vehicles, the weight is saved through the use of lightweight steels, which have reduced the weight of cars by 10% since 1978, without compromising safety [5].

Magnesium offers a greater weight saving capacity than aluminium, as its density, 1.7 g cm^{-3}, is two thirds the density of aluminium, 2.7 g cm^{-3}, without sacrificing strength [6]. However, magnesium has poor creep resistance and this has limited its use to room temperature applications (Table 1).

[1] Kerb weight is defined as the weight of the complete vehicle and all equipment including fuel and water, but without luggage, driver or passengers [1].

Table 1
Magnesium components currently used by car manufacturers.

Component	Car manufacturer	Reference
Hand brake lever	Porsche	[7]
Instrument panel	General Motors, Smart, Buick, Cadillac	[7], [8]
Intake manifold	Diamler Chrysler	[7]
Oil pan	Honda	[7]
Steering wheel	Ford, Lupo, Volkwagen	[7]
Cylinder head cover door	Lupo	[7]
Pedal bracket	General Motors, Ford	[7], [8]
Seat cushion	Smart, Fiat, Jaguar	[7], [8]
Radiator support	General Motors	[7]
Cam cover	Ford	[8]
Grill sections	Pontiac	[8]

Magnesium is the sixth most abundant element on Earth; one cubic mile of sea water contains 6 million tonnes [9]. Despite magnesium being abundant, it has been nearly twice as expensive as aluminium in recent years (Fig. 2). One of the reasons for the high cost is the relatively low demand for magnesium metal. Magnesium is extracted either from ores such as dolomite, magnesite and carnalite or from sea water [7]. The extraction process involves processing the ore or brine to make $MgCl_2$, which is then split by electrolysis to give pure magnesium [7, 10].

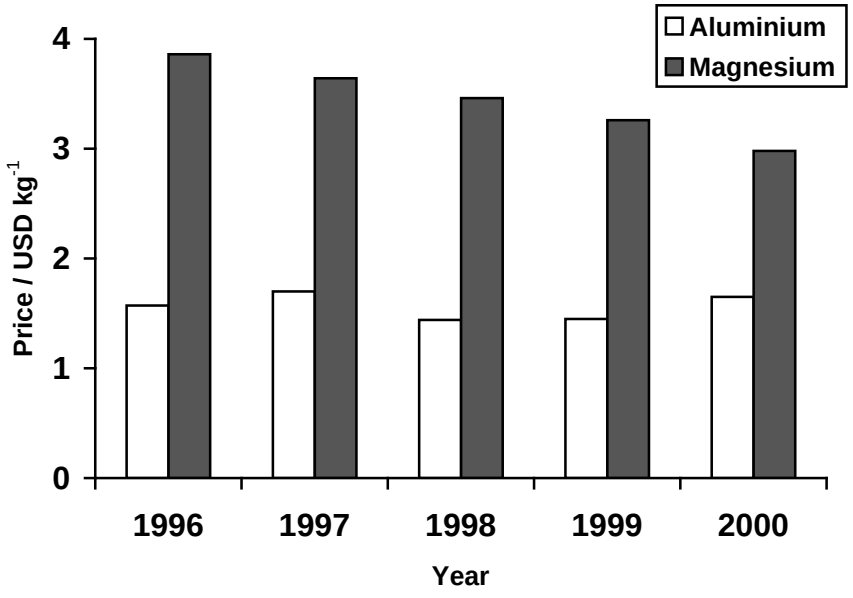

Fig. 2
The price, in US dollars per kg, of aluminium and magnesium ingots over the five years 1996-2000 [11, 12].

The potential for weight saving by using magnesium is about 6%: 77kg for a medium sized car (Fig. 3) [6].

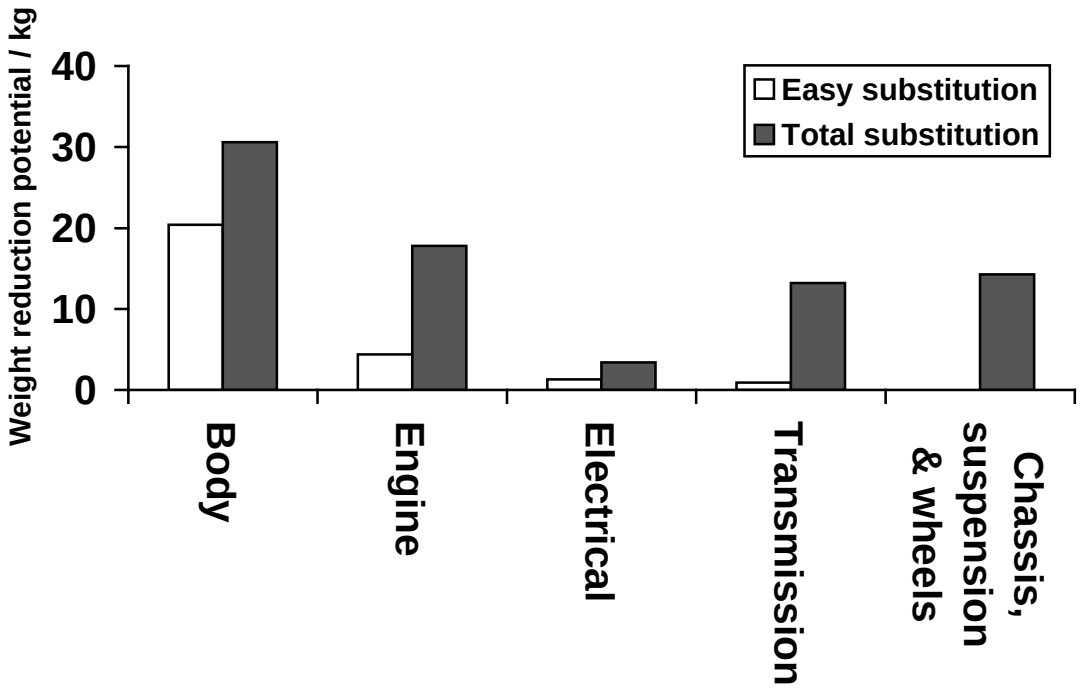

Fig. 3
The potential weight reduction for a medium sized car by the substitution of magnesium alloys whenever possible. A distinction is made between easily achievable substitution and the maximum substitution [6].

The use of magnesium within car engines is limited by stress relaxation[2] causing bolted joints to become loose. In stress relaxation, the initial elastic deformation of the metal becomes a permanent strain over time. The steel bolts used to join sheets of aluminium and magnesium are harder than the metal they hold together. The stress field due to the bolting operation creates elastic strain in the soft metal flanges, which causes Poisson contraction to occur perpendicular to the plane of the flanges. Over time, this elastic deformation becomes a permanent deformation; as the Poisson contraction makes the flanges of aluminium and magnesium thinner in the region close to the bolt (Fig. 4). The distance between the bolt and the nut is fixed and so the joint becomes loose. In a moving vehicle the joint would vibrate, eventually leading to failure.

As the bolts become loose, the problem is compounded by the component starting to vibrate against its fasteners. The joint is considered to be completely relaxed when there is no appreciable force left in the bolt. At this point, the weight of the component will cause the joint to fail completely and the engine will start to fall apart.

[2] A definition of stress relaxation is that, "… it is recognised by a component which is at constant strain under a system of forces, normally below the yield point, showing a time-dependent plastic deformation giving a stress drop with time, the rate of change of stress decreasing with time" [13].

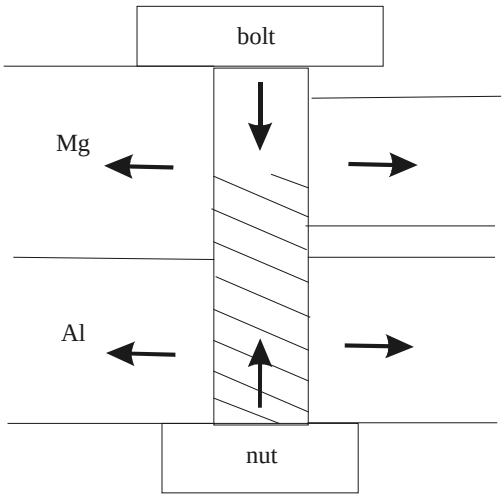

Fig. 4
Diagram showing the forces present in stress relaxation. The left hand side shows the initial forces, while the right hand side shows the magnesium flange relaxing and becoming thinner.

In the remainder of this report I will first of all describe the metallurgy of magnesium and its alloys. Then I shall summarise the current models of stress relaxation before discussing neural networks in detail. Next I will give details of the models that were created. Then I shall describe and discuss the predictions made by the models. Next I will show how the models can be used to reproduce published results and can determine the activation energy of diffusion. Finally, I will draw conclusions from the results.

2 Magnesium

In this section I will discuss the basic metallurgy of pure magnesium. Then I shall discuss the affects of the various alloying elements and summarise the properties of the common magnesium alloys. Next, I will discuss experimental alloys which claim to solve many of the difficulties of using magnesium. I will then discuss the relationship between creep and stress relaxation. Finally, I will discuss the problem of stress relaxation in magnesium.

2.1 Structure and Failure Mechanisms

Pure magnesium has a hexagonal close-packed (hcp) structure (Fig. 5), with a *c:a* ratio of 1.6236, very close to the ideal value of 1.633 for the dense atomic packing of spheres [6]. The principal mechanism by which magnesium alloys may be strengthened is precipitation strengthening, which usually involves aluminium compounds[14].

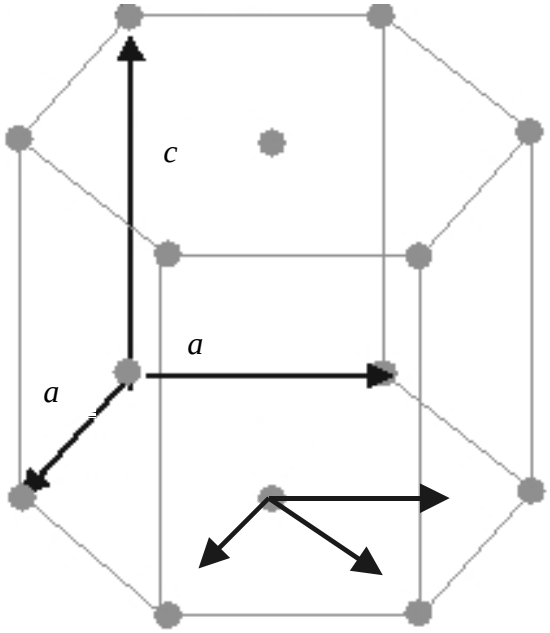

Fig. 5
In a hexagonal crystal, the axes labeled *a* form two sides of a regular hexagon in the horizontal plane. The height *c* is independent of *a*, the *c:a* ratio which describes the atomic spacing of the crystal. The unlabelled arrows show the independent directions of the slip system. For clarity the layer of atoms at *c*/2 has been omitted. This layer is identical to the top and bottom layers that are shown.

At temperatures below 573K, there are only three slip systems, all parallel to the basal plane (0001) (Fig. 5) [15]. Slip occurs when the basal plane is orientated favourably with respect to the applied stress. The slip direction is along the lines of close packed atoms typified by $[11\bar{2}0]$ [6, 16, 17].

The most common magnesium alloy, AZ91D, starts to creep at 100^{o}C and has a maximum service temperature of 125^{o}C [16].

2.2 Magnesium Alloys

Magnesium alloys have been developed for a variety of applications where low density is more important than strength, such as castings for aeroplane components and artificial limbs. Table 2 lists alloy compositions and Table 3 some material costs. The susceptibility of magnesium to creep at relatively low temperatures has limited the variety of its applications, resulting in the development of alloys with higher creep resistance, such as AE42. The potential for thermally activated slip is decreased if alloying elements with low melting temperatures, such as lithium, are excluded from the alloys [6].

Table 2
Alloying elements used in die casting magnesium alloys. The elemental compositions are all given as percentage weight (ASTM B-93) [6]. Rare Earth metals are collectively abbreviated as RE.

Alloy	Al	Zn	Si	Mn	RE	Cu	Fe	Ni	Others
AM20	1.7-2.2	<0.1	<0.1	>0.5		<0.008	<0.004	<0.001	<0.01
AM50	4.5-6.3	<0.1	<0.1	>0.27		<0.008	<0.004	<0.001	<0.01
AM60B	5.7-6.3	<0.20	<0.05	>0.27		<0.008	<0.004	<0.001	<0.01
AS41A	3.7-4.8	<0.10	0.60-1.4	0.22-0.48		<0.04		<0.01	<0.30
AZ91D	8.5-9.5	0.45-0.90	<0.05	>0.17		<0.015	<0.004	<0.001	<0.01
AE42	3.6-4.4	<0.20		>0.27	2.0-3.0	<0.04	<0.004	<0.004	<0.01
ZC63		5.5-6.5		0.25-0.75	1.8-3.0	2.4-3.0			

Table 3
The cost of magnesium alloying elements and the total material cost of some alloys [18]. The dominant cost of magnesium is likely to fall as demand for the metal increases, making the significant factor the cost of the alloying elements.

		AZ91D		AE42	
Alloying element	**Cost ($/kg)**	**Weight of element in alloy (kg)**	**Cost ($/kg)**	**Weight of element in alloy (kg)**	**Cost ($/kg)**
Mg	3.64	0.918	3.342	0.959	3.491
Zn	1.32	0.010	0.013		
Al	1.54	0.092	0.142	0.041	0.063
Rare Earth Elements	15.43			0.033	0.509
	Total materials cost ($/kg)		**3.497**		**4.063**

For the low density properties of magnesium to be preserved, the alloying elements used must also be light. **Aluminium** is often present as it solid-solution strengthens the magnesium, it also improves the castability of the melt and decreases the microporosity of the as-cast alloy. The generic magnesium alloy contains aluminium and consists of two phases:

- α-Mg solid solution
- β-$Mg_{17}Al_{12}$ [6].

The interdendritic β phase has a low melting point [19] and has been shown by Powell *et al.* (2001) to be responsible for the low creep resistance of Mg-Al alloys [20]. There can be as much as 10 vol% $Mg_{17}Al_{12}$ precipitated at the grain boundaries [15]. The motion of dislocations is not restricted to the basal planes as in pure

magnesium [15, 21]. The large quantity of the β phase and the extra slip systems in AZ91D both contribute to the low creep-resistance of the alloy.

The inclusion of **manganese** means that commercial magnesium alloys can possess very high corrosion resistance [9]. Magnesium alloys readily form protective films that prevent corrison from the environment [22]. This is very effective and no alloying element has been found to improve the corrosion resistance [22]. However, galvanic corrosion is a constant threat because magnesium is the most anodic structural metal [9, 22]. The presence of a cathodic metal, such as iron, and any electrolyte, will cause galvanic corrosion to occur [7]. Manganese removes iron impurities from the matrix and forms stable FeMn precipitates [9]. These not only reduce the corrosion rate to below that of mild steel [22], but they also increase creep resistance [6, 23].

Zinc increases strength at ambient temperatures through precipitate-hardening and also increases the fluidity of the melt [5, 23]. The use of zinc is limited to less than 2 wt% to avoid "hot shortness", which occurs when an alloying element with a low melting temperature segregates to the grain boundaries. The material is then likely to separate along its grain boundaries when it is deformed at temperatures close to the melting temperature of the segregated region [24]. Hot shortness increases the brittleness of alloys.

Small quantities of **silicon**, <0.1 wt%, are often added to magnesium alloys because it forms stable silicide compounds with aluminium and zinc, producing precipitates that greatly increase the creep resistance of the alloy [6].

The general properties of magnesium alloys aside from their very high strength-to-weight ratios (Fig. 6, 7) include good castability and machinability (Fig. 8) [9, 10]. Liquid magnesium has low viscosity which enables the casting of large, complicated, thin-walled components; it is possible to cast walls as thin as 0.8mm [9]. The die-casting rate for magnesium alloys can be as much as 25% higher than for aluminium alloys because magnesium, and its alloys, has a low heat capacity [10].

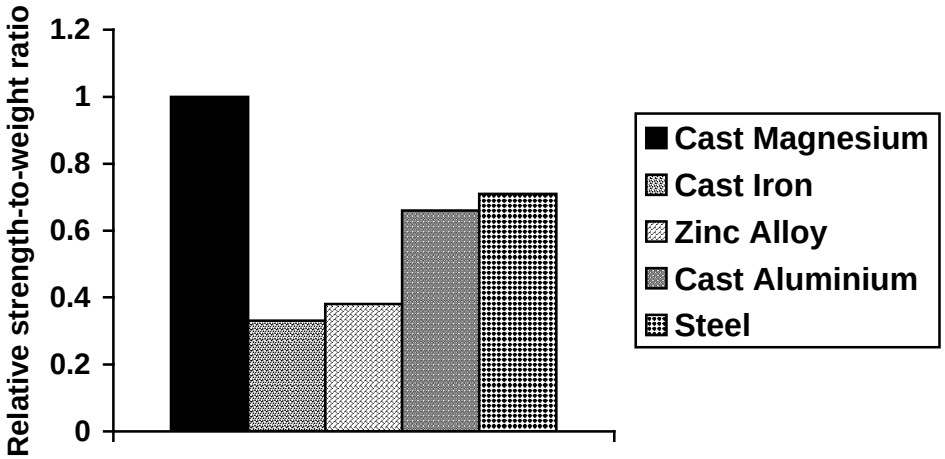

Fig. 6
Strength-to-weight ratios of common structural materials relative to magnesium [10].

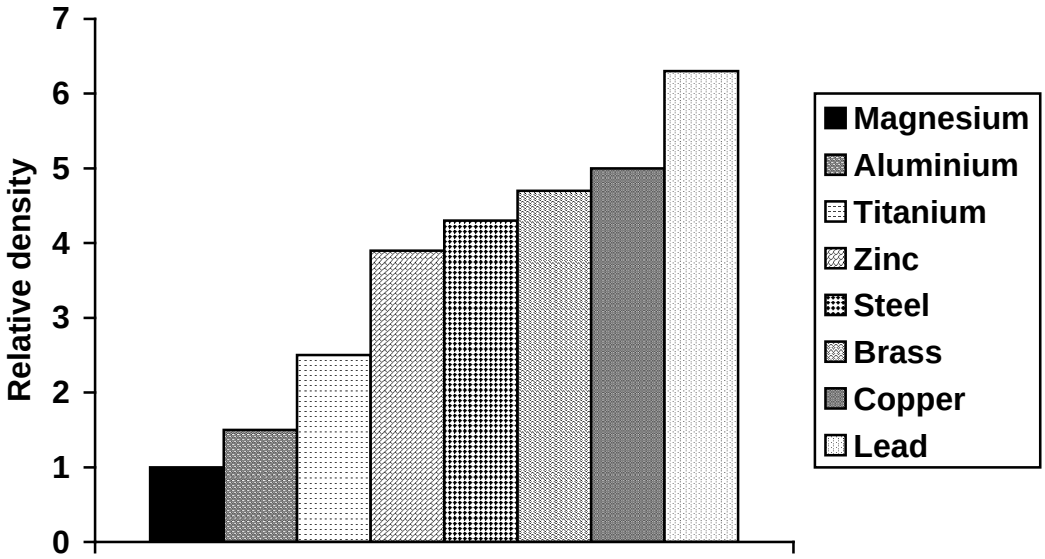

Fig .7
Densities of common structural metals relative to magnesium [10].

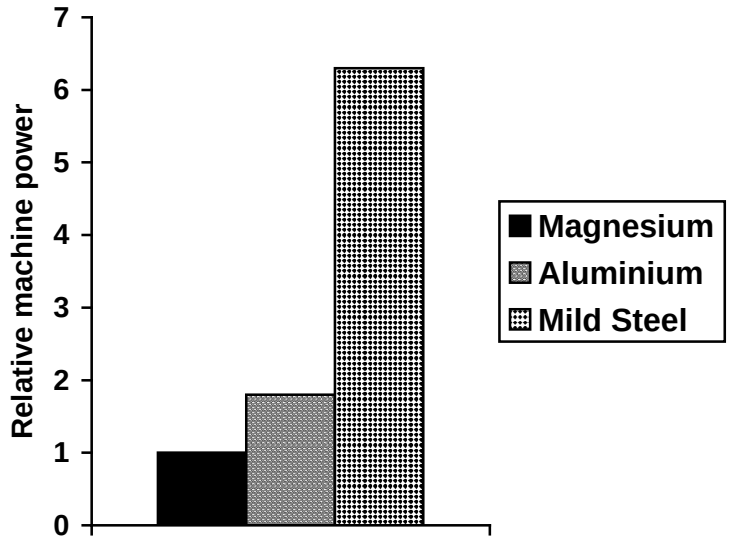

Fig. 8
The machine power needed to perform the same operation on samples of the same geometry and size, of mild steel and aluminium relative to that of magnesium.

The most common magnesium alloy, and by far the cheapest, is designated AZ91D (Table 3, page 6). Its important mechanical properties include high fatigue strength [25], and, initially, relatively good creep strength and stress relaxation resistance [14] (Table 4). However, creep has been observed to occur in AZ91D even at room temperature [26].

Table 4
Comparison of the mechanical properties of AZ91D, the die cast aluminium alloy LM24 and the die-cast zinc alloy BS1004 [9].

Property	**AZ91D**	**LM24**	**BS1004**
Yield strength (MPa)	160	150	-
Tensile strength (MPa)	230	320	283
Compressive yield strength (MPa)	160	-	414
Elongation (%)	3	1-3	10
Hardness (%)	63	80-85	82
Fatigue strength (MPa)	97	138	476
Density (g cm^{-3})	1.81	2.79	6.6

Researchers are also interested in AE42, which contains rare earth elements, and AM20, which has only a small amount of aluminium [6]. These alloys have been developed for improved creep-resistance and are largely responsible for the recent interest in magnesium shown by the automotive industry. Magnesium alloys are now available that have creep resistance similar to that of aluminium alloys. Table 5 gives the creep properties of various magnesium alloys. AS41 has improved creep resistance due to the presence of silicon, which forms $MgSi_2$ precipitates [19]. When the AS41 is die cast, the precipitates are finely dispersed and contribute to creep resistance [19]. The cause of the relatively high creep resistance of AE42 has been subject to some debate [20, 27]. The rare earth elements form $Al_{11}RE_3$ precipitates, which are only stable below 150^{o}C; at higher temperatures they decompose into Al_2RE, Al_4RE and $Mg_{17}Al_{12}$ [20].

Table 5
Creep coefficients for AZ91D, AS41A and AE42 at 100^{o}C and 100MPa using the two power law formalism $\varepsilon_p = at^b$ and $\varepsilon_s = c + dt$ where ε_p = primary creep strain and ε_s = secondary creep strain, t = time and a, b, c and d are constants found by regression [28]

Alloy	*a*	*b*	*c*	*d*
AZ91D	0.078	0.45	0.280	0.0028
AS41A	0.036	0.65	0.116	0.0021
AE42	0.042	0.40	0.117	0.0003

.
The cost of AE42 makes it too expensive to use in automobiles and alternatives with lower costs are currently being developed. Several alloys based on the Mg-Al-Ca system (ACX alloys) have been investigated for creep-resistance [29]. The experimental ACX alloys have considerably 25% higher creep resistance than AE42 [29, 30]. A strontium containing subgroup of the ACX alloys have shown high potential for power-train components at the same cost of manufacture as AZ91D [30]. ACX alloys containing zinc, ZAC alloys, have been found to be slightly cheaper than AZ91D and to outperform both AZ91D and AE42 in applications below 150^{o}C [31]. The ZAC alloys also have slightly more creep resistance than A380, the industry standard alloy for power-train components [31].

The alloys described above are unsuitable for use in their current form for various reasons: ACX alloys have been unable to die-cast reliably and ZAC alloys have exhibited extreme sensitivity to composition [32]. Norada A and Norada N alloys, have been developed to meet the need for a creep resistant magnesium alloy [28].

The published results seem promising, but the compositions of these alloys have not yet been released [28].

All this exciting work developing new and better alloys has lead to older alloys, such as AZ91D, being abandoned by researchers. It is possible that the full potential of AZ91D in automotive design has not been realised. The purpose of this project is to be able to predict how stress relaxation will proceed in AZ91D. This will enable engineers to make full use of this alloy.

2.3 Creep and Stress Relaxation

Mechanical tests used to quantify both creep and stress relaxation measure the strain rate sensitivity of the material. Paetke (1980) has shown that these quantities are the same, and hence that creep is equivalent to stress relaxation [13]. If a bolt is tightened onto a component, the total strain on the shank is constant. However, the initial elastic strain created by the applied stress can be replaced over time by inelastic, or creep strain [31]. The accumulation of inelastic strain causes the stress to relax.

Since there is little literature dealing explicitly with stress relaxation, we shall now consider stress relaxation as a form of creep. The creep rate is limited by diffusion, which is temperature dependent [31]. Creep is generally thought of as a high temperature phenomenon, but the homologous temperature, T/T_m, where T is the temperature and T_m is the melting temperature, is a useful indicator for when creep occurs [14]. AZ91D has a tendency to creep at low temperatures as indicated by its relatively high T/T_m of 0.46 [14, 27].

Creep behaviour can be divided into three stages: primary, secondary, or steady-state, and tertiary. In the middle steady-state stage, the strain rate, $\dot{\varepsilon}$, is described by :

$$\dot{\varepsilon} = \mathrm{A}\sigma^n e^{-Q/RT} \qquad (1)$$

where σ = initial stress, Q = activation energy for diffusion, T = temperature, R = molar gas constant, 8.314 J K^{-1} mol^{-1} and A, n are materials constants [31].

This expression has been empirically derived from creep data using a)
a graph of strain rate against logarithmic stress shows power law dependence (Fig. 9).

$$\Rightarrow \dot{\varepsilon} = B\sigma^n \qquad (2)$$

and b)

a plot of logarithmic strain rate versus inverse temperature has gradient $-\frac{Q}{R}$ (Fig. 10).

$$\Rightarrow \dot{\varepsilon} = Ce^{-Q/\ RT} \qquad (3)$$

By combining expressions (2) and (3), equation (1) is obtained [31].

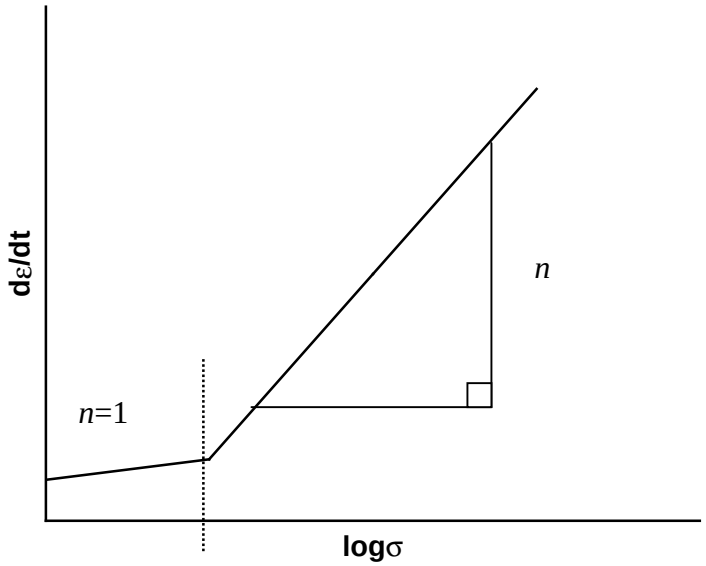

Fig. 9
Graph of strain rate versus logarithmic stress used to derive (2). Typically, $n \approx 3-8$.

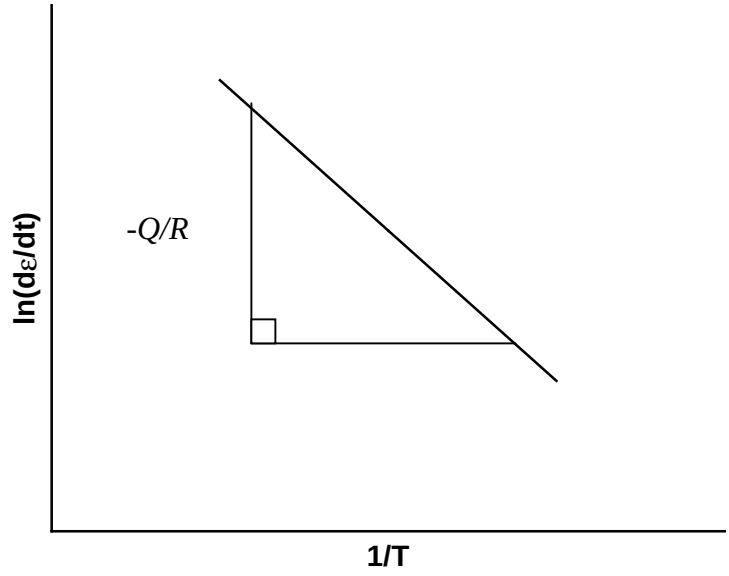

Fig. 10
Graph of logarithmic strain rate versus inverse temperature used to derive (3).

There are several creep mechanisms which include dislocation (power law) creep and diffusional (linear-viscous) creep.

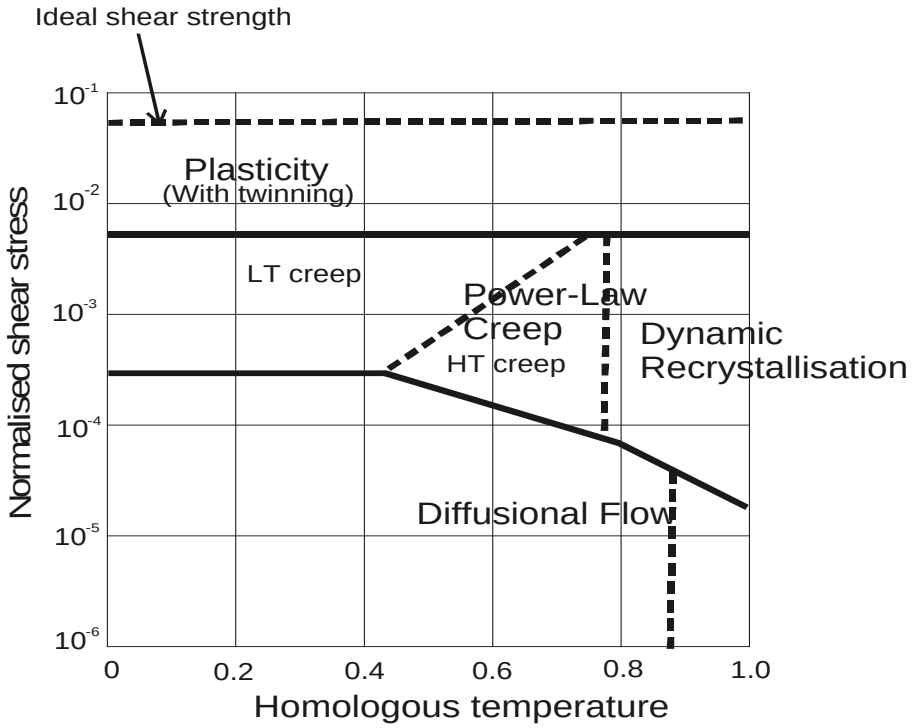

Fig.11
Deformation mechanism map for pure magnesium with a grain size of 0.1 mm [32]. LT creep and HT creep are low and high temperature creep, respectively.

At small stress levels, diffusion creep is the dominant mechanism (Fig. 11). The applied stress acts as a driving force for diffusion through the grains and is relieved by grain elongation. For high homologous temperatures, as in the case of magnesium, bulk diffusion through the crystal lattice occurs [31].

At large stress levels, and at temperatures greater than $0.3T_m$, dislocation creep occurs. When a precipitate blocks the path (ie pins a dislocation) there is often a component of the glide force which creates a climb force, which tries to push the dislocation out of its slip plane. The dislocation can only move upwards if the atoms in the plane below it are able to diffuse away. The climb unpins the dislocation from the precipitate, allowing further slip to occur. Dislocation climb has been found to be the rate-controlling dislocation reaction for magnesium based alloys at temperatures below 150^{o}C [6, 23, 26]. In pure magnesium, the movement of dislocations is restricted to the basal planes, while in alloys, such as AZ91, the presence of precipitates causes climb to occur [23]. $Mg_{17}Al_{12}$ precipitate grows on the basal planes, causing pinning and promoting dislocation climb. The hardening mechanism changes during this process from solid solution hardening to precipitation hardening [23]. Creep will occur when the amount of precipitate exceeds a certain level, and therefore the creep rate is dependent on the amount of supersaturated alpha-magnesium [23].

3. Summary of Models in Current Use

In this section I will review the models currently used to simulate stress relaxation.

Several models for creep and stress relaxation have been developed which are based on the motion of dislocations [13]. However, researchers have not yet been able to develop an analytical model of stress relaxation or of creep. There are a large number of variables involved, such as details of the composition, microstructure, temperature, time, and applied force. Such a large number of variables suggests that this problem is one too complicated for theorists to solve completely. The models currently in use are based on a mixture of the understood theory and empirical techniques.

Magnesium is a brittle material and so the primary stage of creep has relatively small duration. Cavitation growth, which marks the onset of tertiary creep, does not occur if the sample is in compression, in which case there is no tertiary creep [16]. Secondary creep is widely accepted as the only relevant creep process and all the models focus on it. Experiments have shown that steady-state creep of magnesium obeys the conventional power law (1) [21]. Researchers in steel have produced various empirical models for stress relaxation and creep, the general forms of which should be applicable to magnesium alloys.

A two parameter creep equation has been used successfully by Ellis *et al*. (2000) to model stress relaxation in stainless steel [33]. This is given by:

$$\frac{\varepsilon}{\varepsilon_r} = 1 - \left(1 - \left(\frac{t}{t_r}\right)^{(m+1)}\right)^{\delta} \tag{4}$$

where ε = strain, ε_r = strain to rupture, t = time, t_r = time to rupture and m, δ are material constants.

This dimensionless equation amounts to strain being proportional to time, in some power law determined by the material [33]. Despite the physical underpinning of this equation, it is an empirical equation; the constants m and δ are determined using regression analysis.

Similar power laws, based similarly on strain being proportional to time, include

$$\varepsilon = \alpha \log t + \beta \tag{5}$$

where α and β are constants that depend on the applied stress [34] and

$$\varepsilon_p = at^b;\ \varepsilon_s = c + dt \tag{6}$$

where ε_p = primary creep strain and ε_s = secondary creep strain [26, 35]. These approaches are very similar to each other in that they are all regression analyses. The only advantage of one over another would appear to lie within the data set being considered i.e. one data set might be closer to (5) than (6). The regression analysis performed to obtain (5) used an exponential function in its fitting. The analysis used to obtain (6) divided the data into two regions before performing a regression on each

part. The primary creep strain was found to be best fitted by a power law and the secondary strain by a linear relationship. This is contrary to the results of Ashby *et al*. (1982), which suggest a power law relationship for secondary creep [31].

Equations (4) to (6) are limited in scope to cases where the bolt and the material being bolted have similar thermal expansion coefficients. This is not the case for the bolting of magnesium, or aluminum, by steel bolts. Differing thermal expansion coefficients will create differing distributions of stress as temperature changes. Various authors have considered this problem and have developed a compliance-based approach [36, 37, 38]. Compliance is related to stiffness in the following way:

$$[S_{ij}] = [C_{ij}]^{-1} \tag{7}$$

where S_{ij} is the stiffness matrix and C_{ij} is the compliance matrix.
It is often easier for engineers to measure and calculate the compliance and so it is a substitute for stiffness.

As for (4) to (6) the compliance approach is empirical, as there is no physical justification for the compliance to be the only determining factor in stress relaxation. The dependence of compliance on time is given by

$$F(t) = F_0\left(\frac{C^f + C_0^b}{C^f + C^b(t)}\right) \tag{8}$$

where $F(t)$ = residual force in bolt, F_0 =initial force, C^f = compliance of fastener, C^b_0 = initial compliance of bolt and $C^b(t)$ = compliance of bolt at time t.

A more complicated expression considering thermal expansion has recently been derived from the dimensions of the fastener [16].

$$\begin{aligned} F(T) &= F(T_0) + \frac{(T - T_0)}{K}\left(\alpha_{Mg} l_{Mg} + \alpha_w l_w + \alpha_b l_b\right) \\ K &= \frac{l_b}{A_b E_b} + \frac{l_w}{A_w E_w} + \frac{l_{Mg}}{A_{Mg} E_{Mg}} \end{aligned} \tag{9}$$

where the subscripts *Mg*, *W* and *b* refer to magnesium, washer and bolt respectively, α = thermal expansion coefficient, l = length, A = stressed area, E = Young's modulus and $F(T)$ = residual force at temperature T .

4 Neural networks

The problem of stress relaxation is a complicated one. The movement of dislocations during stress relaxation has been studied and various theories developed, but no analytically consistent method [13, 40]. The number of variables involved means that to produce an empirical model, assumptions, based on known mechanisms, need to be made, for example that the strain rate has a power law dependence [41]. A linear regression model is likely to be inadequate since generalisation beyond the data set is known to be poor because there is no justification for linearity [42, 43]. A more general regression technique is a neural network [44, 45].

Mathematically, a neural network may be described by the mapping

$$\boldsymbol{x} \rightarrow \boldsymbol{y}\,(\boldsymbol{x}; \boldsymbol{w}, \mathsf{A}) \tag{10}$$

where the parameters defining the physical problem form the input vector $\boldsymbol{x}$, the

vector $\boldsymbol{w}$ contains the weights and A describes the architecture of the network [43, 44]. A neural network requires a minimum of three layers: input, hidden (of which there may be more than one) and output [42]. Each input is connected to all the units in the hidden layer; the set of connections formed by each input is called a neuron (Fig. 12) [41]. The connections in the hidden layer are each assigned a weight and there are also weights on the connections between hidden layers and between the final hidden layer and the output. Initially the weights are randomised, and then during the

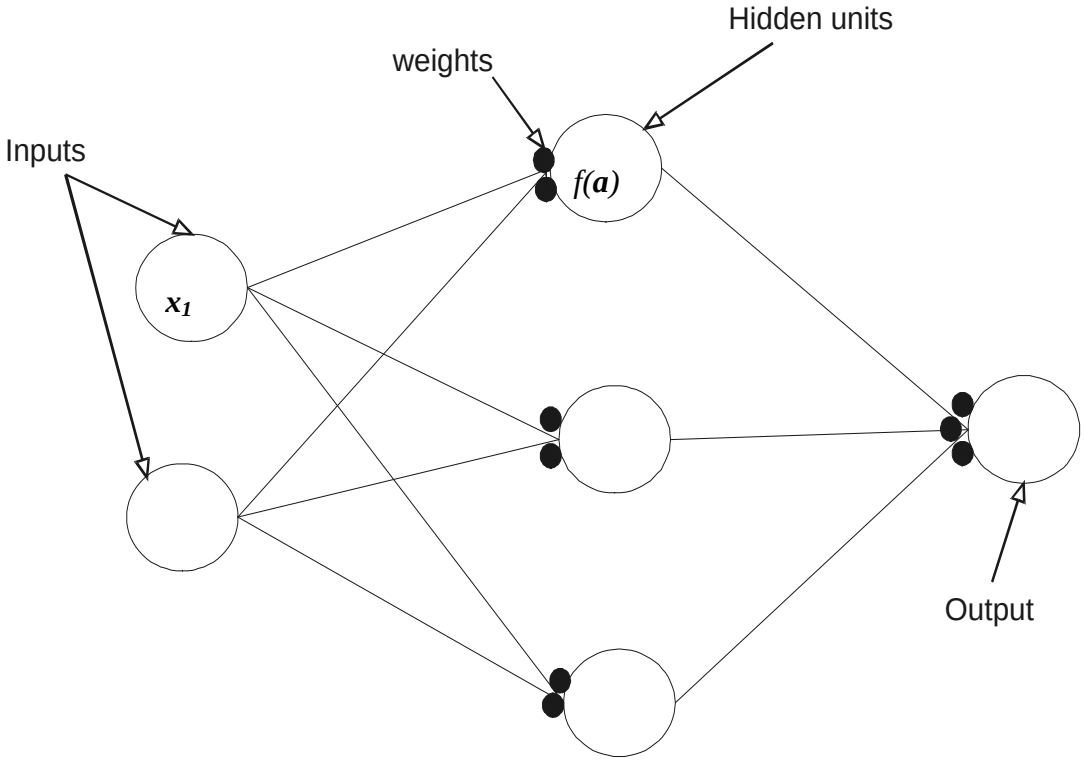

creation of the model a learning algorithm optimises the weight vector so that the objective function is minimised [41, 42, 43, 44, 46].

Fig. 12

Schematic diagram of a neural network with two inputs, $\boldsymbol{x_1}$ and $\boldsymbol{x_2}$. The function $f(\boldsymbol{a})$ is applied in the hidden units and the function $y(\boldsymbol{a})$ is applied at the output neuron.

The objective function in this case is the sum squared error:

$$E_D(\boldsymbol{w}) = \frac{1}{2}\sum_m \sum_i \left(t_i^{(m)} - y_i\left(\boldsymbol{x}^{(m)}; \boldsymbol{w}\right)\right)^2 \tag{11}$$

where m = current set of data points, $t_i^{(m)}$ = ith component of the target vector (the known value which the output of the network should reproduce); $y_i\left(\boldsymbol{x}^{(m)}; \boldsymbol{w}\right)$ = ith component of the output vector as function of the input vector, $\boldsymbol{x}$, and the weight vector, $\boldsymbol{w}$ [44, 46].

To favour small values of $\boldsymbol{w}$, and thus avoid overfitting the model [44], the objective function is often modified to:

$$M(\boldsymbol{w}) = E_D\beta + E_W\alpha \tag{12}$$

where $E_W = \frac{1}{2}\sum_i w_i^2$, and α, β are constants [44, 46].

The hidden layer is not just concerned with the application of weights to the inputs. Here a, usually, non-linear function is applied to the input [41, 42, 44, 46]. The output is produced as a combined effect of the hidden unit functions on the inputs. If the weights have been correctly optimised an output function of any form can be simulated by overlaying many functions in the hidden units. A popular choice of function is the hyperbolic tangent since it any curve can be reproduced by a combination of them (Fig. 13) [41]. This may be represented mathematically as:

$$a_j^{(1)} = \sum_l w_{jl}^{(1)} x_l + \theta_j^{(1)} \qquad h_j = f^{(1)}(a_j^{(1)}) \tag{13}$$

$$a_i^{(2)} = \sum_j w_{ij}^{(2)} h_j + \theta_i^{(2)} \qquad y_i = f^{(2)}(a_i^{(2)}) \tag{14}$$

where x_l = lth component of input vector $\boldsymbol{x}$, w = weights, θ = biases (a random value drawn from a Gaussian distribution), h_j = output of jth hidden layer and y_i = ith component of output vector $\boldsymbol{y}$. For example, $f^{(1)}(a)$= tanh(a) and $f^{(2)}(a)=a$ [44].

The process of optimising the weights is often referred to as "training the network". This is done using half of the data (the training dataset). The weights are adjusted until the predicted output is close to the real output [43]. The remaining data are used to test the model. As training progresses, the model is able to fit the training dataset with increasing accuracy. Whilst the error on the training data should decrease as the complexity of the model increases, the error on the test set should reach a minimum value before starting to increase (Fig. 14) [43, 44, 46]. It is possible for the model to become so complex that it starts to model the noise in the data rather than the underlying physical trend [43, 46]. This is one of the hazards of using nonlinear methods such as neural networks and is known as "overfitting" [41, 44, 46]. When the test error begins to increase, the model is as complicated as it needs to be to model the data but training continues in order to create a committee [43]. The committee is

used to avoid overfitting by including the "best" parts of various submodels[3]. The poor predictions made by a submodel are ignored in favour of better predictions made by other submodels.

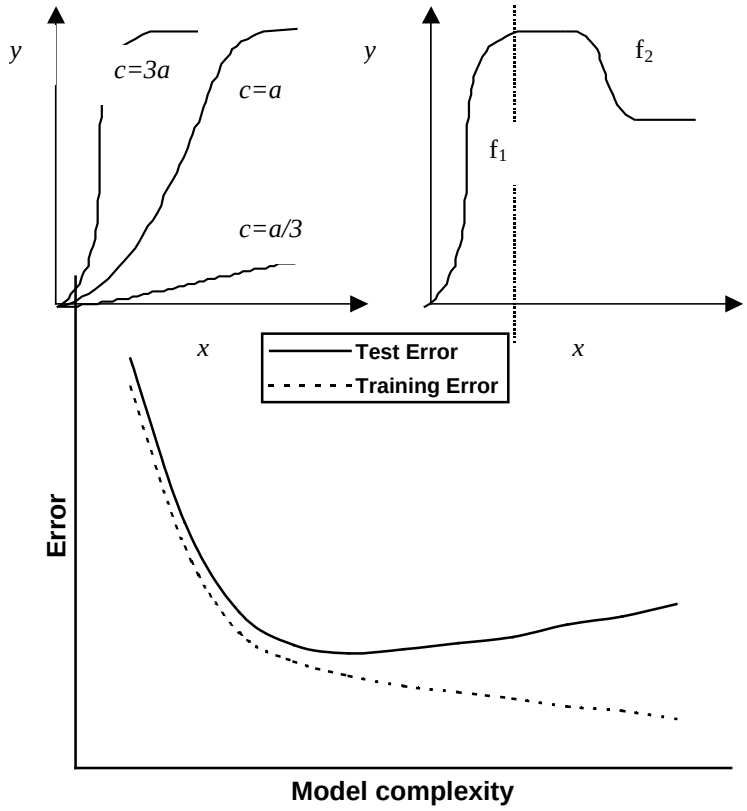

Fig. 13 Sketches showing the flexibility of single tanh curves. The graph on the left shows the functions $y = \tanh(cx)$ for various c, the graph on the right shows a combination of tanh curves given by $y = f(x)$ where $f_1 = c\tanh(cx)$ and $f_2 = d + \tanh(-dx)$

[3] Here a submodel is one small network generated from one set of weights and random values. The term model refers to a committee model, made from several submodels that are amalgamated into the committee so that the best parts of each model are preserved, but the poorer parts have little influence over the output.

Fig. 14
Comparison of test error and training error as model complexity increases [44, 46]

The complexity of the model may be described by the number of submodels that it contains. Despite the fact that the submodels may contain different numbers of hidden units, it is usually the case that two submodels are more complicated than one. Therefore the number of submodels used to form a committee can be determined from a plot of the test error. To make this plot, the errors of the individual submodels are amalgamated to form the Combined Test Error (CTE) [44, 46]. The optimum number of submodels is the one with the minimum value of test error.

To choose the best submodels to go into the committee, the submodels are ranked by either increasing Test Error (TE)

$$\text{TE} = E_D(\boldsymbol{w}) = \frac{1}{2}\sum_m \sum_i \left(t_i^{(m)} - y_i\left(\boldsymbol{x}^{(m)}; \boldsymbol{w}\right)\right)^2 \tag{15}$$

or decreasing Log Predictive Error (LPE)

$$\text{LPE} = \sum_i \frac{1}{2}\frac{\left(t^{(m)} - y^{(m)}\right)^2}{\sigma_y^{(m)2}} + \log\sqrt{2\pi\sigma_y^{(m)}} \tag{16}$$

where σ_y = perceived noise in the relevant submodel [44, 46].

MacKay has shown that the traditional use of TE may be misleading and that LPE is a better measure of prediction accuracy [44, 46].

All the models created were based on the Bayesian approach to neural networks developed by MacKay [44, 46, 47], in which information about uncertainty is included through the use of Bayes' theorem [46]. Practically, this means that the models make predictions with error bars that show the error in fitting the model, ie the uncertainty in the model. The error bars shown in subsequent graphs show the combined fitting error and the perceived noise.

5 The Models

In this section I will discuss the data from which the models were created. Next I will describe how the models discussed in Section 3 can be used with a neural network. Finally I shall give the details of the construction of each model.

The database used for creating the models contained the following variables:

- temperature
- torque used to tighten the bolt before the experiment began
- stiffness of the bolt
- initial force on the bolt
- area under the flange of the bolt and in contact with the AZ91D
- time

The output of the models is the residual force in the bolt, as a function of the above variables.

The distribution of the experimental data is shown in Fig. 15. It shows where the models will produce predictions with small errors. Certain variables were restricted to specific values, for example three sizes of bolt were used, with three flange areas. This is why the information space for some of the variables appears to be discrete.

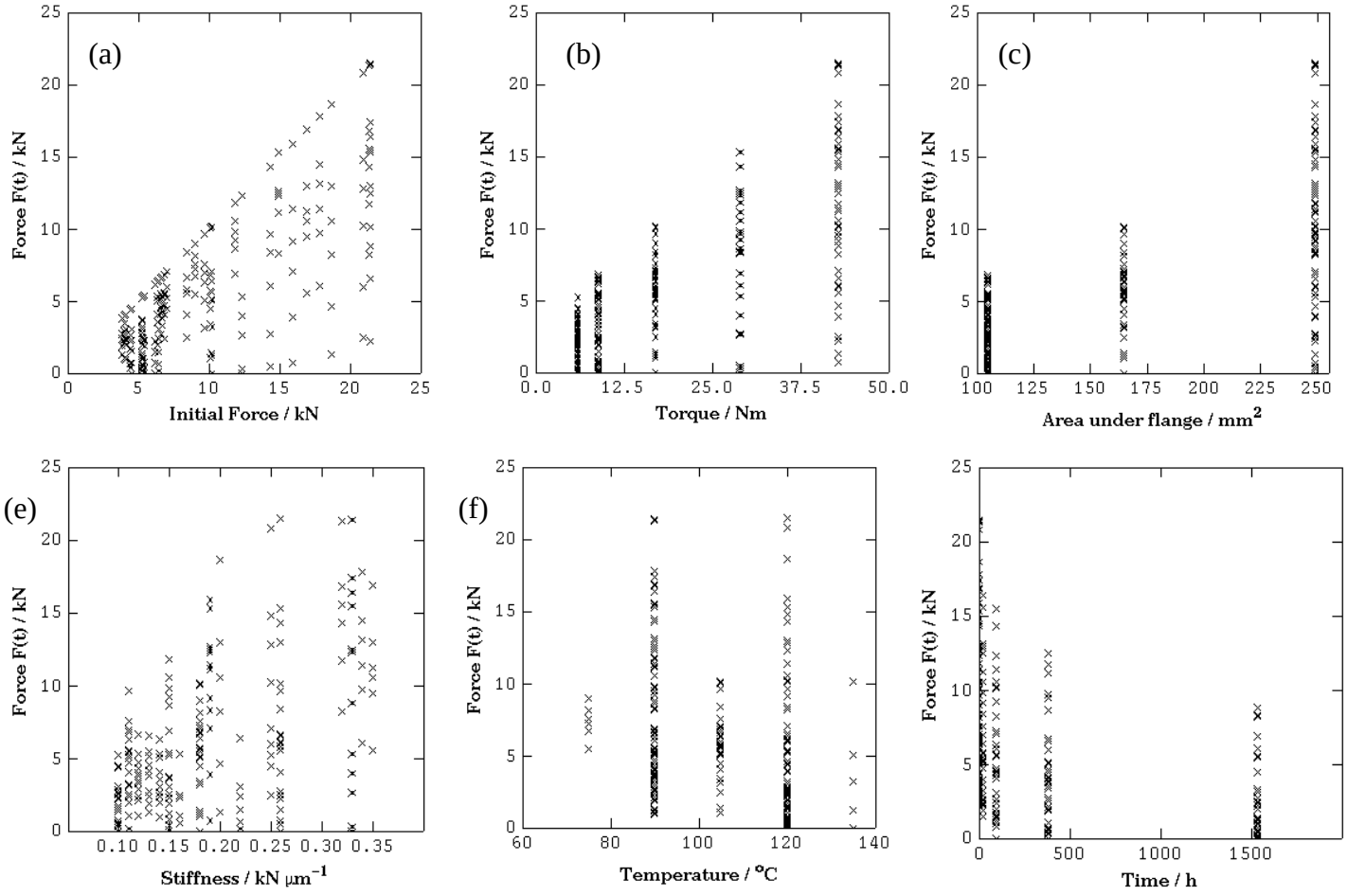

Fig. 15

Graphs showing the information space in the original database as used to create the models. The graphs show the measured force against (a) initial force, (b) torque, (c) area, (d) stiffness, (e) temperature and (f) time.

The following models were created:

- Model 1 using the original database
- Model 2 using the original data and diffusion equation inputs
- Model 3 using only the diffusion equation inputs
- Model 4 using inputs based on the empirical compliance approach.

The equation for steady state creep,

$$\dot{\varepsilon} = \mathrm{A}\sigma^{n} e^{-Q/RT} \tag{1}$$

includes the influence of diffusion on the creep process [31], but is an equation for strain rate, which was not in the original database. Integrating this equation to give an expression for the strain as a function of temperature and time, suggested the physical inputs of *1/T*, $\ln\sigma$ and $\ln t$.

$$\dot{\varepsilon} = \frac{d\varepsilon}{dt} = A\sigma^{n} e^{-Q/\ RT}$$

$$\therefore \varepsilon = tA\sigma^{n} e^{-Q/\ RT} \tag{16}$$

$$\therefore \ln\varepsilon = \ln t + \ln A + n\ln\sigma - \frac{Q}{RT}$$

In order to ensure that the best possible model was created, these "diffusion" inputs were added to the original data to create Model 2 and were used alone to create Model 3. In doing this it was possible that Model 2 would be biased, but it may also reveal relationships in the data that were unsuspected.

The expression for compliance was taken from the work of Yang *et al*. [37], which shows that the force present in the bolt can be written in terms of the "bolt compliance"

$$F(t) = F_0\left(\frac{C^{f} + C_0^{b}}{C^{f} + C^{b}(t)}\right) \tag{7}.$$

where $F(t)$ = residual force in bolt, F_0 =initial force, C^f = compliance of fastener, $C^b{}_0$ = initial compliance of bolt and $C^b(t)$ = compliance of bolt at time *t*.

Bolt compliance is defined as the ratio of the deformation of the bolt to the applied load [37], and as such is related to stiffness.

$$C^{f} = \frac{\sum T_{flange}}{AE} \tag{17}$$

where T_{flange} = thickness of the flanges clamped by the bolt, A = bolt area, E = Young's modulus of bolt.

Fitting a power function of the form $\alpha + t^{m}\beta$ to the creep curve produced by the experimental data gives the following expression for the creep strain of the bolt:

$$\varepsilon(t) = \alpha + t^{0.2}\beta \tag{18}$$

Hence, the time dependent compliance term can be expressed as

$$C^b(t) = \frac{T_h}{A}\left(\alpha' + t^{0.2}\beta'\right) \tag{19}$$

where α' and β' are $\frac{\alpha}{\sigma}$ and $\frac{\beta}{\sigma}$.

Then (7) can be approximated by $C \sim \frac{t^{0.2}}{A}$ (20)

[37, 38[4]]. The inverse of C is used as an input to Model 4. Therefore Model 4 actually has two stiffness inputs.

The inputs to the various models are shown in Tables 6 and 7.

Table 6
Shows which inputs were used for each model and the units used.

Input	Units	Model 1	Model 2	Model 3	Model 4
Temperature	^{o}C	✓	✓		✓
Torque	N m	✓			
Stiffness	kN μm^{-1}	✓	✓		✓
Initial Force	kN	✓	✓		✓
Area	mm^2	✓	✓		
Time	h	✓	✓		
1/T	K^{-1}		✓[5]	✓	
lnσ	kN mm^{-2}		✓	✓	
Lnt	h		✓	✓	
1/C	h$^{0.2}$ mm^{-2}				✓

Table 7
A basic statistical analysis of the database used to create the models. The very large standard deviations correspond to inputs with discrete information spaces. The units are as before.

	Temperature	Torque	Stiffness	Initial Force	Area	Time
Minimum	75	6	0.10	3.84	105	0
Maximum	135	43	0.35	21.5	249	1536
Mean	105	19.97	0.19	10.3	166.37	341
Standard Deviation	15.21	14.3	0.08	5.72	63.74	550.59

[4] There is some disagreement over the exponent Chen *et al*. (1997) use 0.3 [38] whereas, Yang *et al*. (1999) use 0.2 [37]. The use of 0.2 in this work was decided by the toss of a coin.
[5] Units of ^{o}C^{-1} were used to allow consistency within Model 2.

5.1 Model 1

Model 1 displayed a clear minimum value for its CTE at nine submodels (Fig. 16). The submodels were chosen to maximise LPE and the largest σ_v value (perceived noise) of any of the submodels was 0.11468. This is less than half the experimental error of 0.23 (Appendix C).

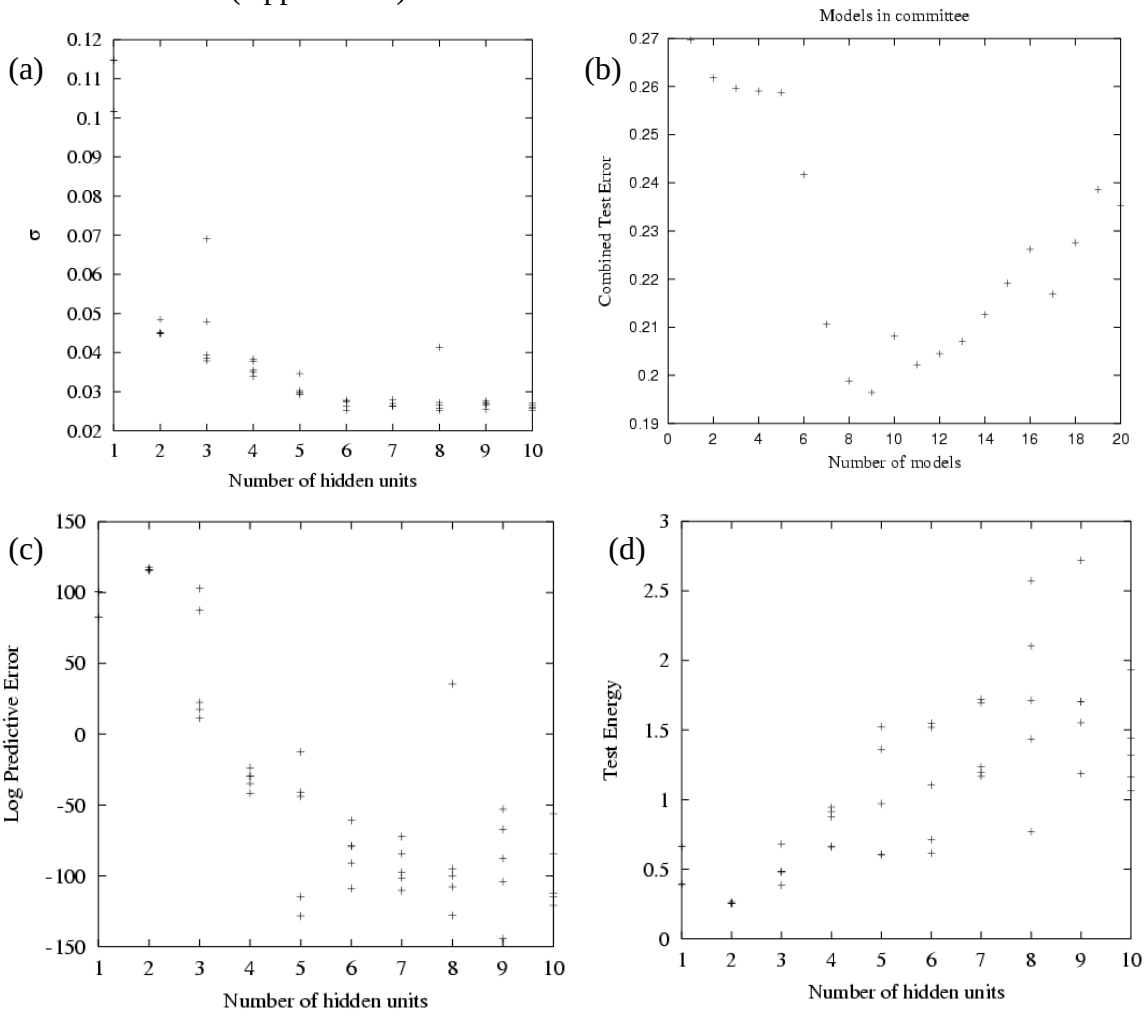

Fig. 16
The graphs used to determine the size of the committee of submodels for Model 1: (a) perceived noise (σ) vs number of hidden units; (b) CTE vs number of models; (c) LPE vs number of hidden units; (d) TE vs number of hidden units.

A maximum of 10 hidden units was used when creating Model 1. It was found that increasing the number of hidden units to 20, as done for the other models, resulted in exactly the same committee.

The model was tested by predicting the results given in the experimental database. The graph of predicted force versus actual force (Fig. 17) shows that almost all the error bars of the data points intersect the line of the perfect model: predicted result equals experimental result.

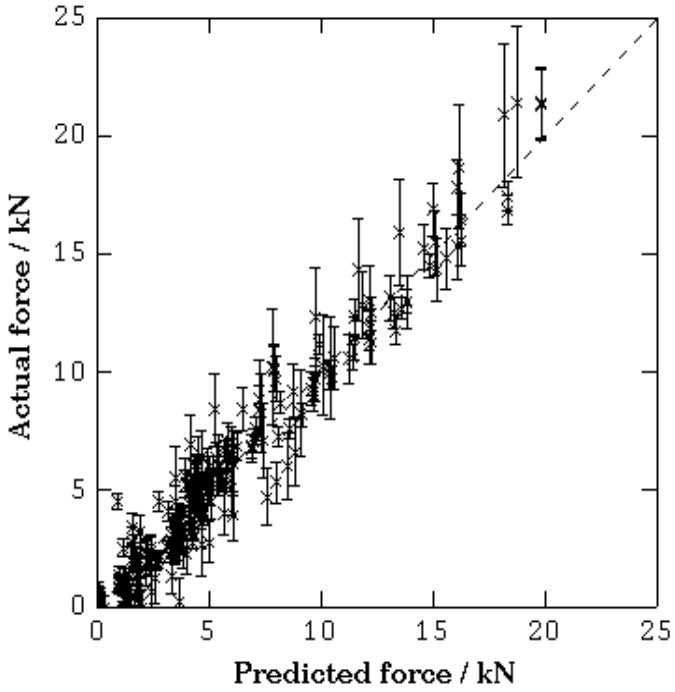

Fig. 17
Graph of actual, or experimentally measured, force versus force predicted by Model 1. The dashed line shows the perfect correlation of predicted = actual. This is a committee prediction using the entire original dataset. The error bars represent a combination of the fitting error and σ_v.

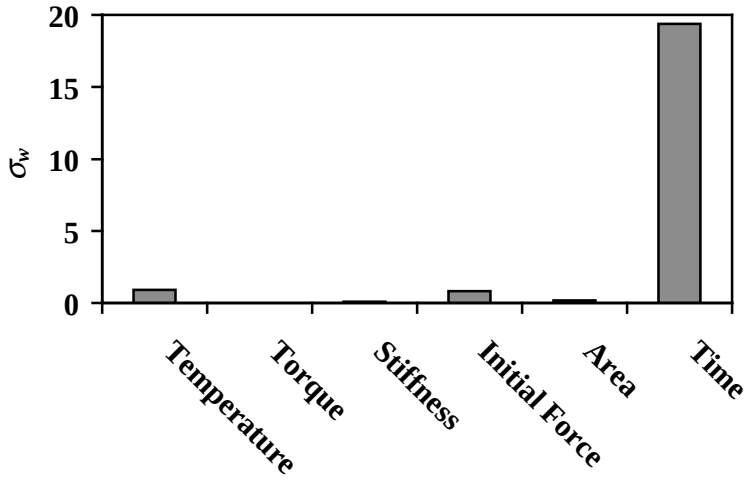

Fig. 18
Bar graph showing the relative significance, $\sigma_{w,}$ of the inputs to Model 1.

The relative significance of the individual inputs can be determined from the weights [47]. These values should support the physical theories of stress relaxation; time and temperature should be the most important factors in determining the amount of stress relaxation. The time was by far the most significant input; it was nearly 20 times more significant than any of the others (Fig. 18). Temperature and starting force were also significant which agrees with the basic creep equation (1) because the stress involved is the initial stress, closely related to initial force. Torque was almost

completely insignificant as expected. It would have been very surprising if the residual force had been dependent upon how the bolt was tightened. The very small significance of torque, lead to it being omitted from subsequent models.

Model 2

Model 2 has an increasing function for its CTE (Fig. 19), so only one submodel was chosen. The perceived noise (0.02269) was much lower than that of Model 1.

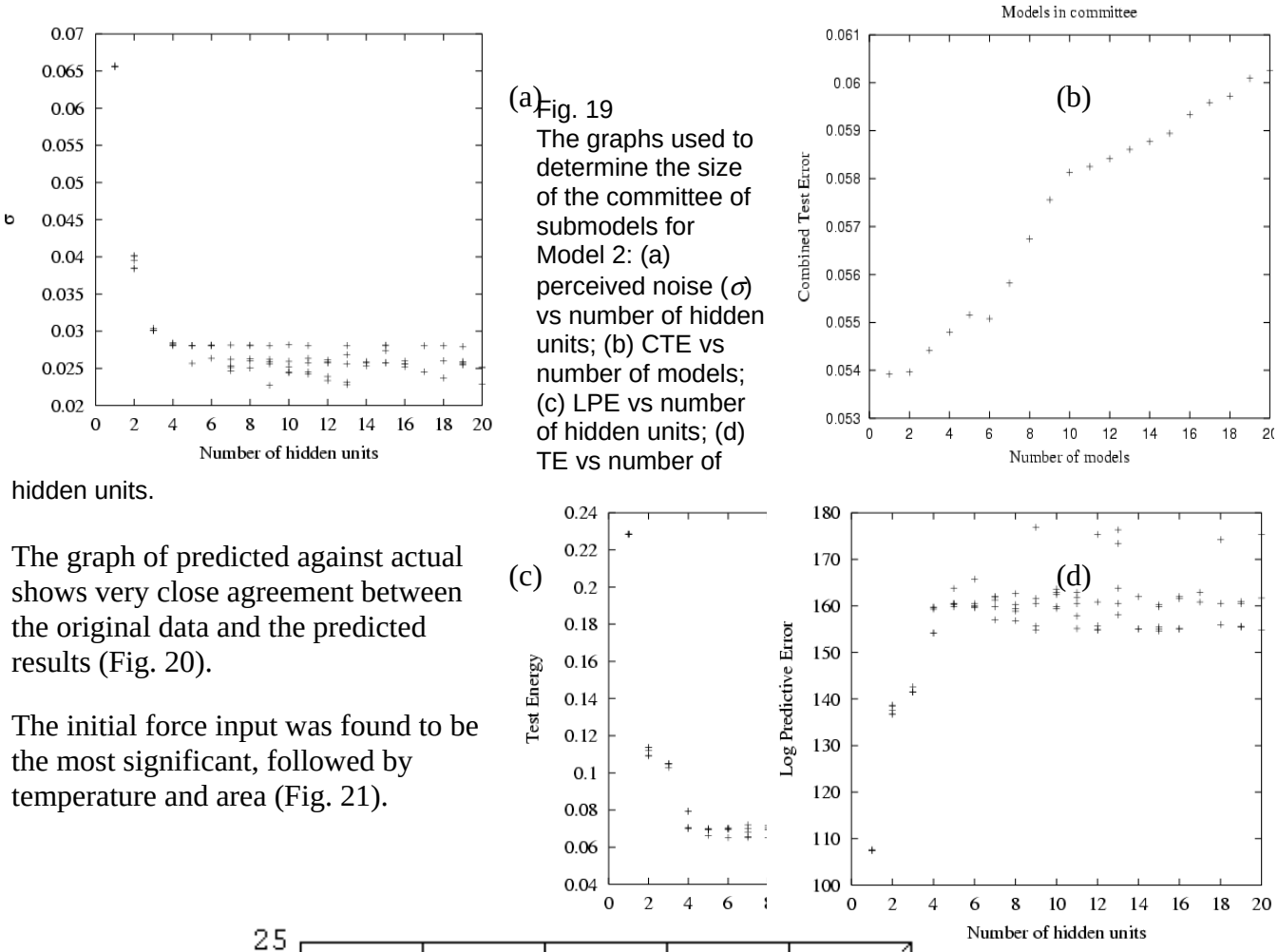

Fig. 19
The graphs used to determine the size of the committee of submodels for Model 2: (a) perceived noise (σ) vs number of hidden units; (b) CTE vs number of models; (c) LPE vs number of hidden units; (d) TE vs number of hidden units.

The graph of predicted against actual shows very close agreement between the original data and the predicted results (Fig. 20).

The initial force input was found to be the most significant, followed by temperature and area (Fig. 21).

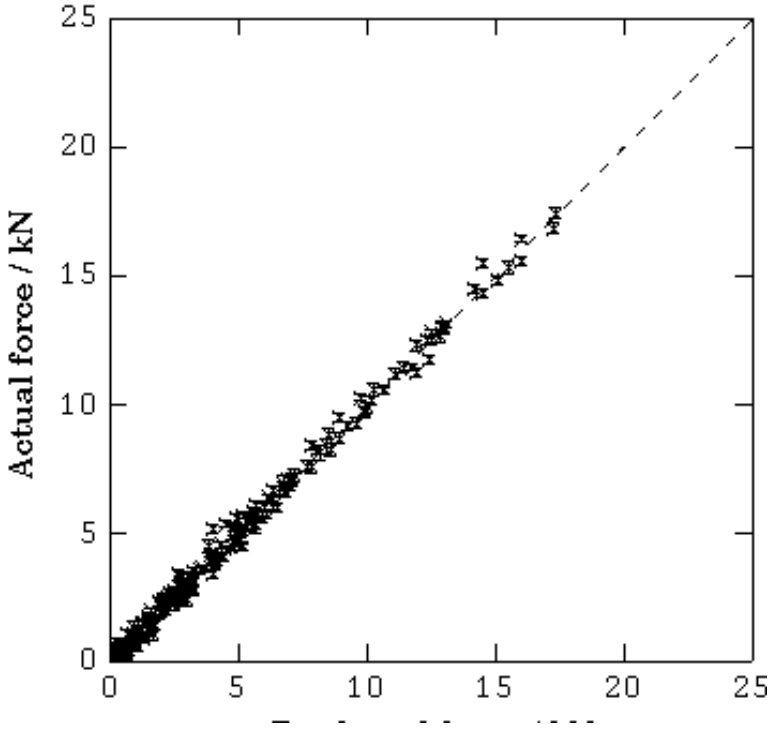

Fig. 20
Graph of actual, or experimentally measured, force versus the force predicted by Model 2. The dashed line shows the perfect correlation of predicted = actual. This is a committee prediction using the database used to create this model. The error bars represent a combination of the fitting error and σ_v.

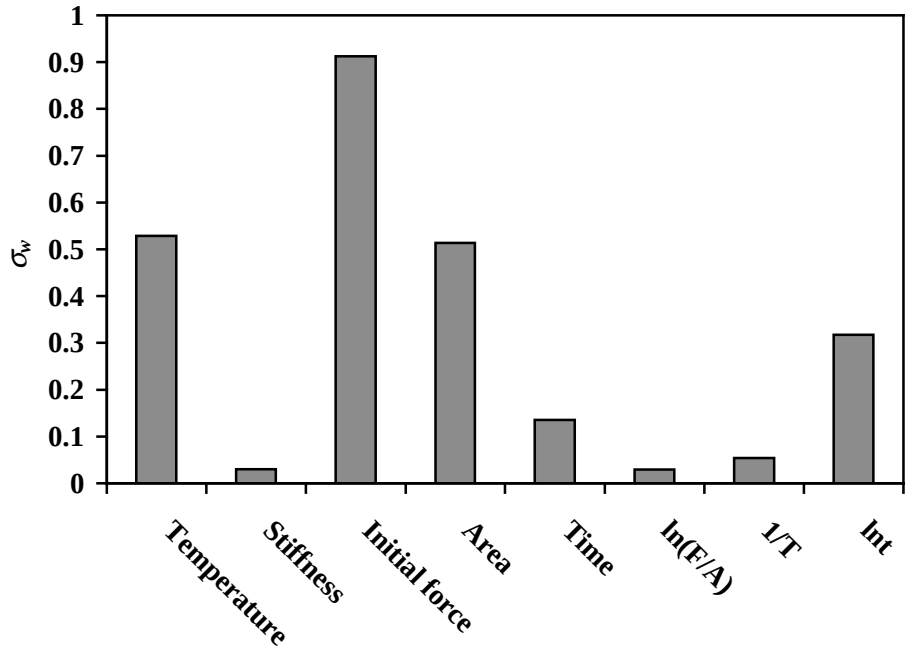

Fig. 21 Bar graph showing the relative significance, σ_w, of the inputs to Model 2.

At first sight, the difference in the significance of time between Model 1 and Model 2 is surprising. However, the σ_w values are not measuring the sensitivity of the output on the input, they are partial correlation coefficients. This means that it is not correct to directly compare the σ_w values. A more scientific method for comparing models to use both models to make the same prediction and to compare the results, both with each other and with accepted physics.

It is clear that the initial force and the clamping force are highly likely to be proportional. Model 1 makes such a prediction but Model 2 makes a very strange prediction (Fig. 22).

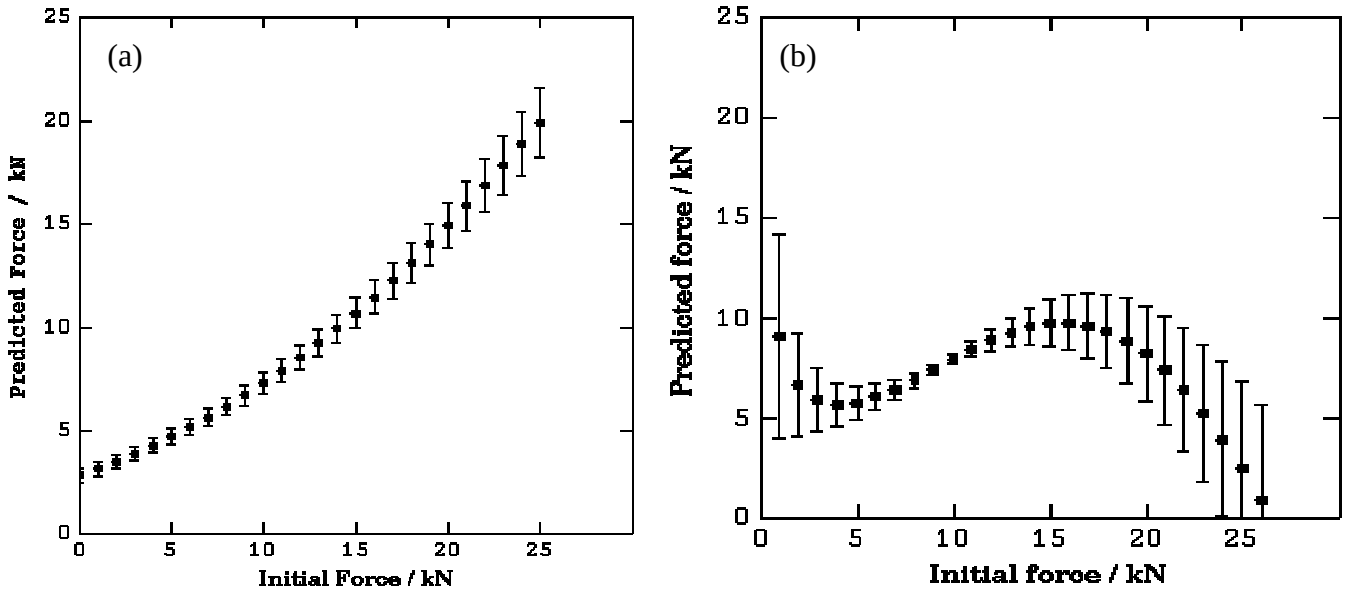

Fig. 22
Comparison of the predictions made by Model 1 and Model 2 for the affect of varying the initial force. Graph (a) shows the prediction of Model 1, which is almost the line $y = x$, as expected. Graph (b) shows the prediction of Model 2, which is clearly unphysical. The error bars represent a combination of the fitting error and σ_v.

There are three possible reasons for the poor behaviour of Model 2: it could be a poor model or biased or overfitted. Introducing physical inputs may produce a better model, but they may also bias the model by obscuring "hidden" relationships within the data in favour of relationships that scientists predict. Overfitting occurs when the model fits the data too closely and starts to model the experimental noise rather than the underlying physical trend. It is not clear whether Model 2 is biased or overfitted but this model is unphysical. I think that the very small level of noise supports the proposition that this model is overfitted. There was no further development of this model.

5.3 Model 3

Model 3, like Model 2, has an increasing function for its CTE (Fig. 23). The perceived noise (0.1243) was slightly greater than that of Model 1.

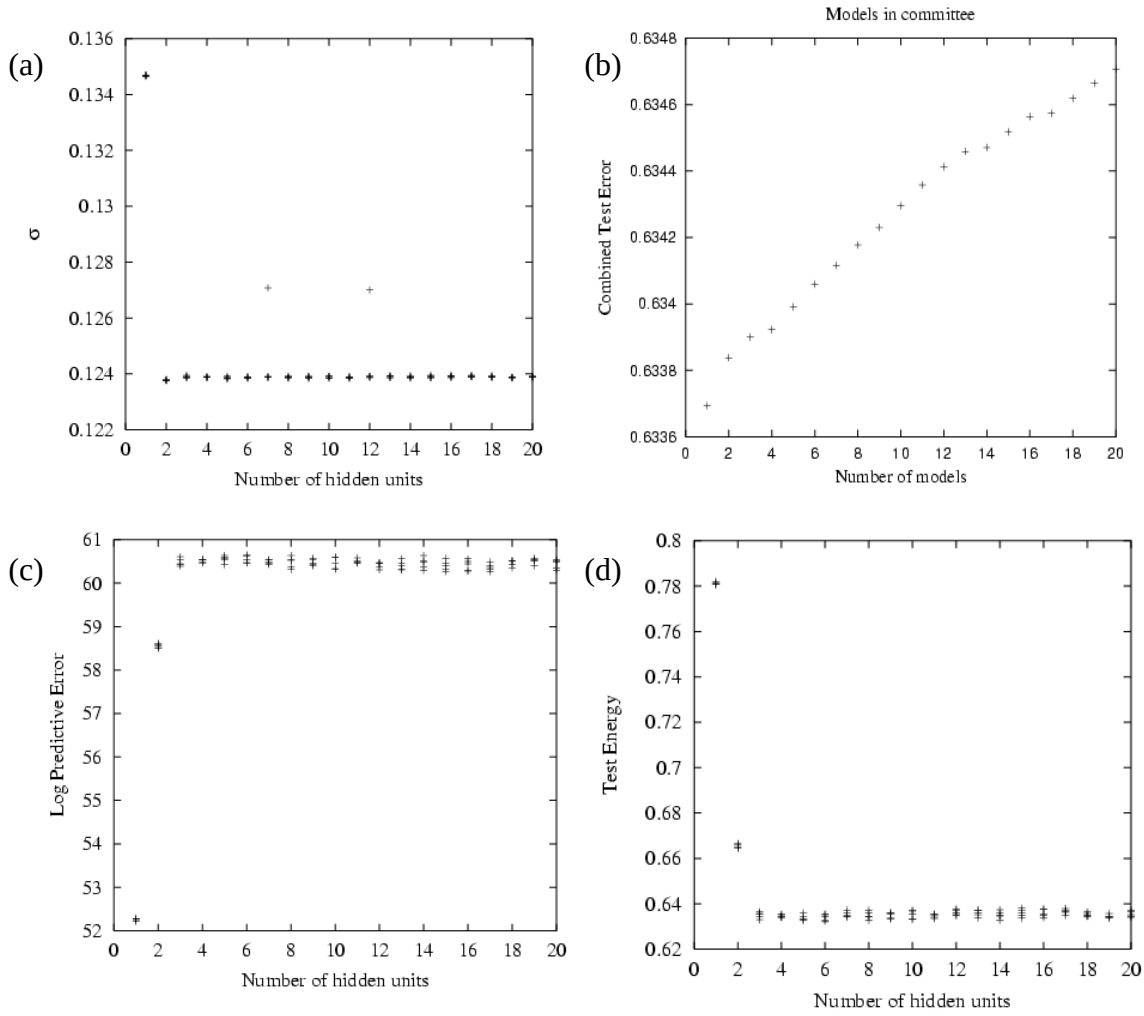

Fig. 23
The graphs used to determine the size of the committee of submodels for Model 3: (a) perceived noise (σ) vs number of hidden units; (b) CTE vs number of models; (c) LPE vs number of hidden units; (d) TE vs number of hidden units.

The correlation between predicted and actual force is low; the extent of the error bars is not sufficient to explain the large amount of scatter away from the line $y = x$ (Fig. 24).

The initial stress term was found to be the most significant, and was more than twice as significant as the time input which was more than twice as significant as the inverse temperature (Fig. 25).

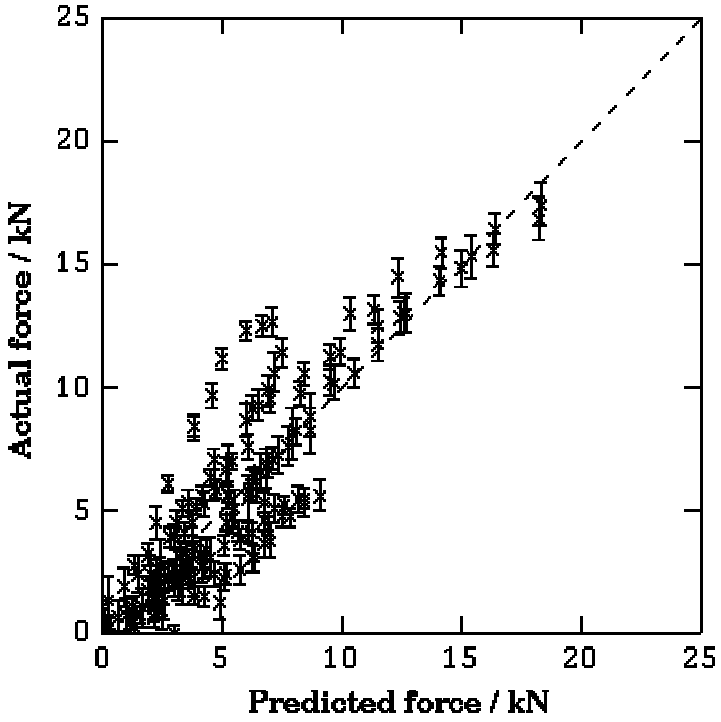

Fig. 24
Graph of actual, or experimentally measured, force vs the force predicted by Model 3. The dashed line shows the perfect correlation of predicted = actual. The error bars represent a combination of the fitting error and σ_v.

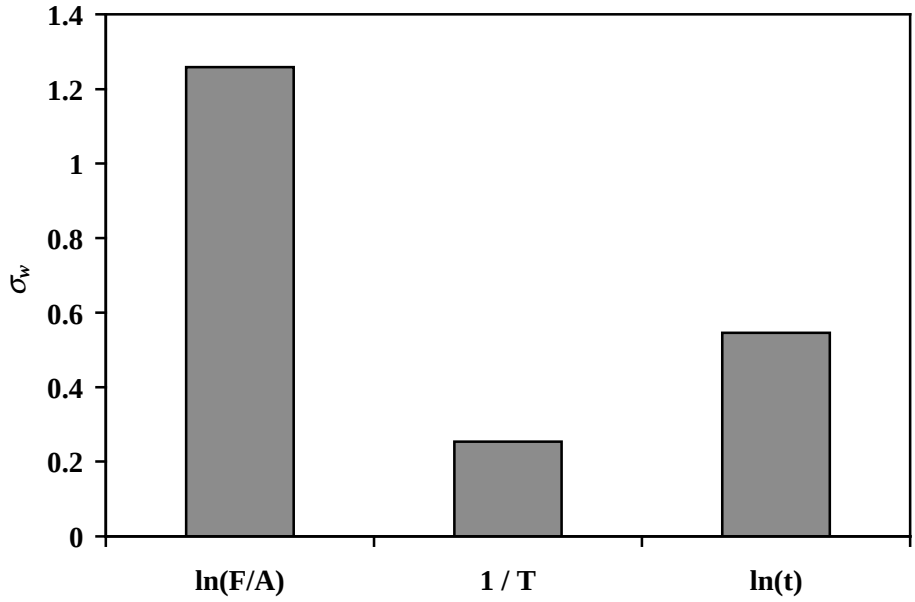

Fig. 25
Bar graph showing the relative significance of the inputs to model 3.

5.4 Model 4

The CTE of Model 4 is

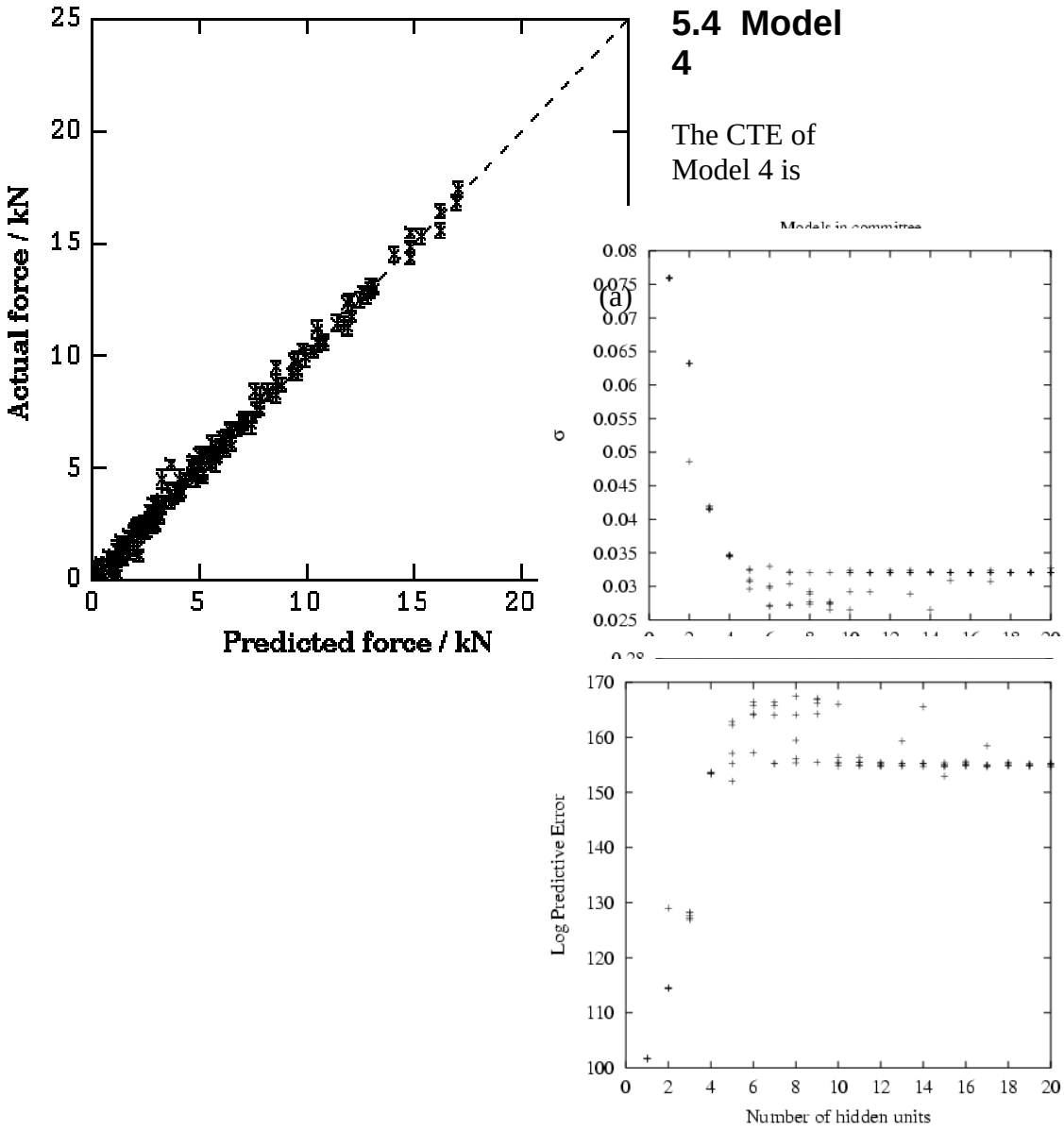

minimised by 17 submodels, making this model more complicated than the other three (Fig. 26). The perceived noise (0.03097) was much lower than that of Model 1.

Fig. 26
The graphs used to determine the size of the committee of submodels for Model 4: (a) perceived noise (σ) vs number of hidden units; (b) CTE vs number of models; (c) LPE vs number of hidden units; (d) TE vs number of hidden units.

The predicted versus actual force graph shows very close agreement between the original data and the predicted results (Fig. 27).

The initial force input was found to be the most significant, followed by compliance and temperature (Fig. 28). This is reminiscent of Model 2, but the trends produced by Model 4 appear to be physical (Fig. 29).

(d)

Fig. 27
Graph of actual, or experimentally measured, force vs force predicted by Model 4. The dashed line shows the perfect correlation of predicted = actual. The error bars represent a combination of the fitting error and σ_v.

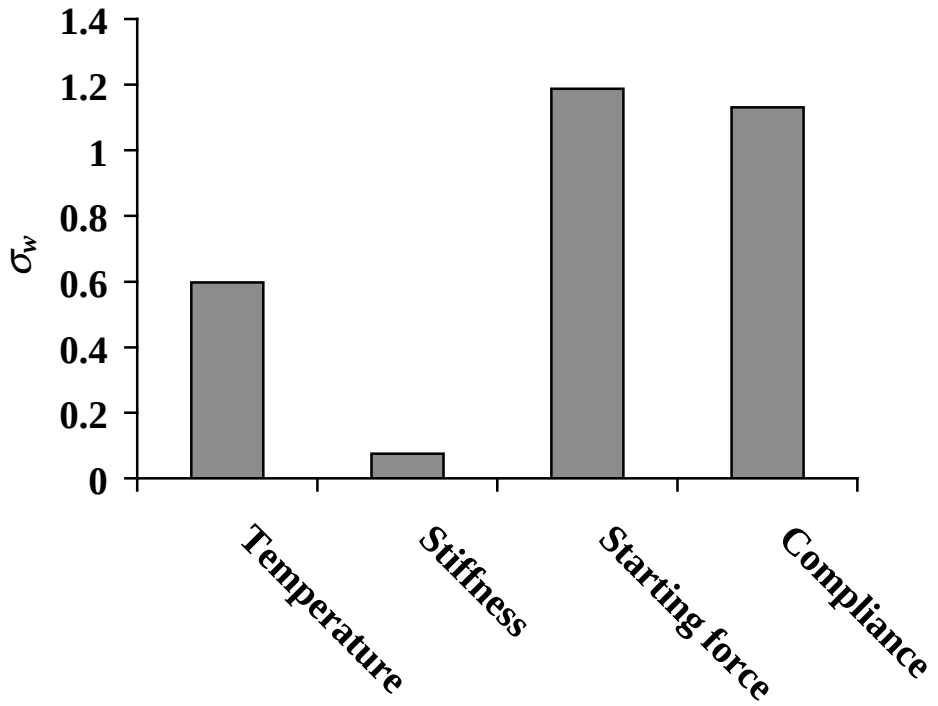

Fig. 28
Bar graph showing the relative significance of the inputs to Model 4.

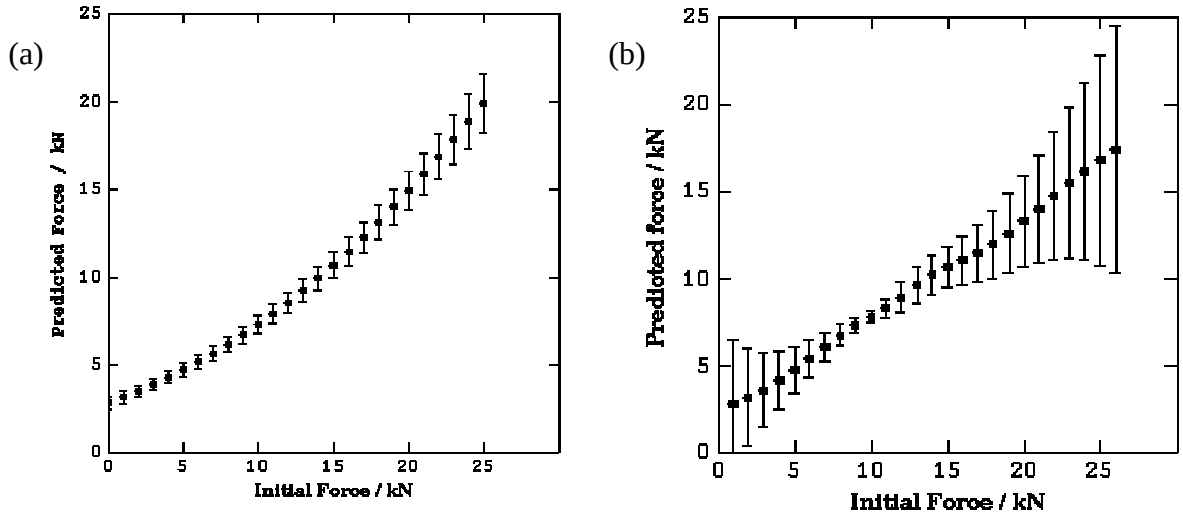

Fig. 29
Comparison of the predictions made by Model 1 and Model 4 for the affect of varying the initial force. Graph (a) shows the prediction of Model 1, which is almost the line $y=x$, as expected. Graph (b) shows the prediction of Model 4, which contains more uncertainty but also follows the same physical trend. The error bars represent a combination of the fitting error and σ_v.

The obvious extension of the project, a model with the same inputs as Model 3 but with stiffness added, was disappointing. The perceived noise was slightly lower than in the case of Model 3, but the predictions had huge levels of uncertainty. The cause of this is unknown and the model was abandoned.

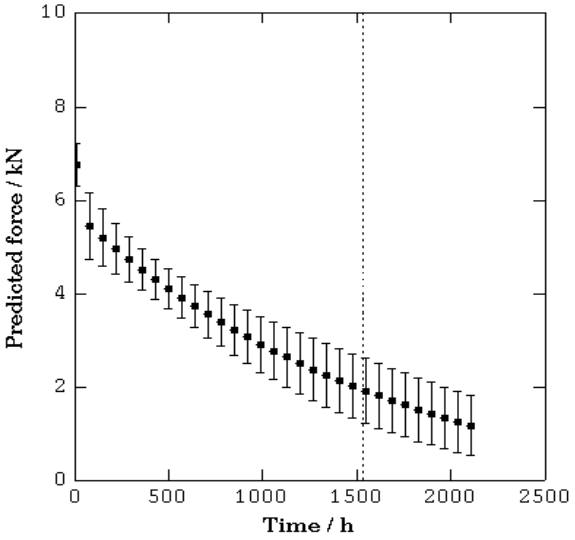

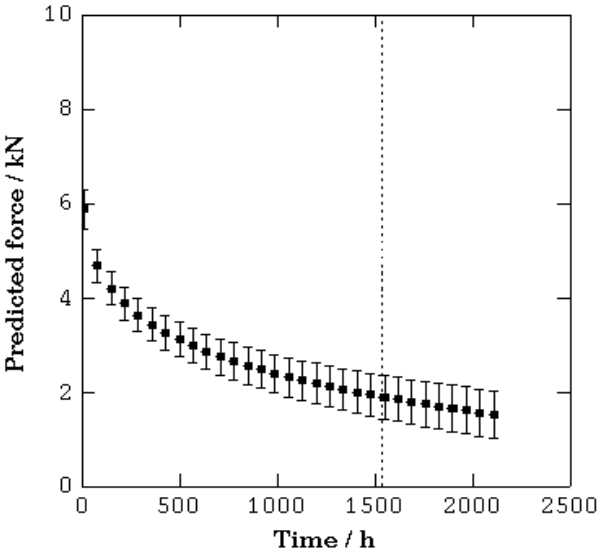

Model 1 Model 3

caution as a performance upper bound.

6.1 Time

Engineers wanting to use magnesium components in a car engine are most interested in the performance of the bolted joints as a function of time. The trends produced by all three models show the expected decrease in force as time increases (Fig. 30). The error bars are small and do not increase significantly beyond the edge of information space. This indicates that the relationship between force and time is modeled well. The disparity between the magnitudes of the predicted forces shows that each model has a different functional relationship between force and time. The predictions made by Model 1 and Model 2 agree, although Model 2 is less uncertain than Model 1. The prediction made by Model 4 is significantly higher than those of Models 1 and 2. Also the force appears to be approaching a limit greater than zero. These facts suggest that Model 4 has not made a physical prediction.

At the start of the experiment the bolt is strained elastically. This strain is gradually converted to plastic strain as the creep process begins. The effect of this is an elastic shortening of the flanges and the bolt shaft [37]. The magnitude of this effect has been shown to be small and has been neglected without compromising the results obtained [37]. The results of Albright *et al*. (1991) show that the residual stress in the bolt decreases rapidly and does not reach a linear regime until five hours have passed [48]. This is consistent with the rapid decrease in force predicted by all models (Fig. 20). The time-force curve predicted by Model 3 is the same shape as examples found elsewhere in the literature [48, 49]. The prediction made by Model 1 is almost linear and the prediction made by Model 4 approaches the wrong limit.

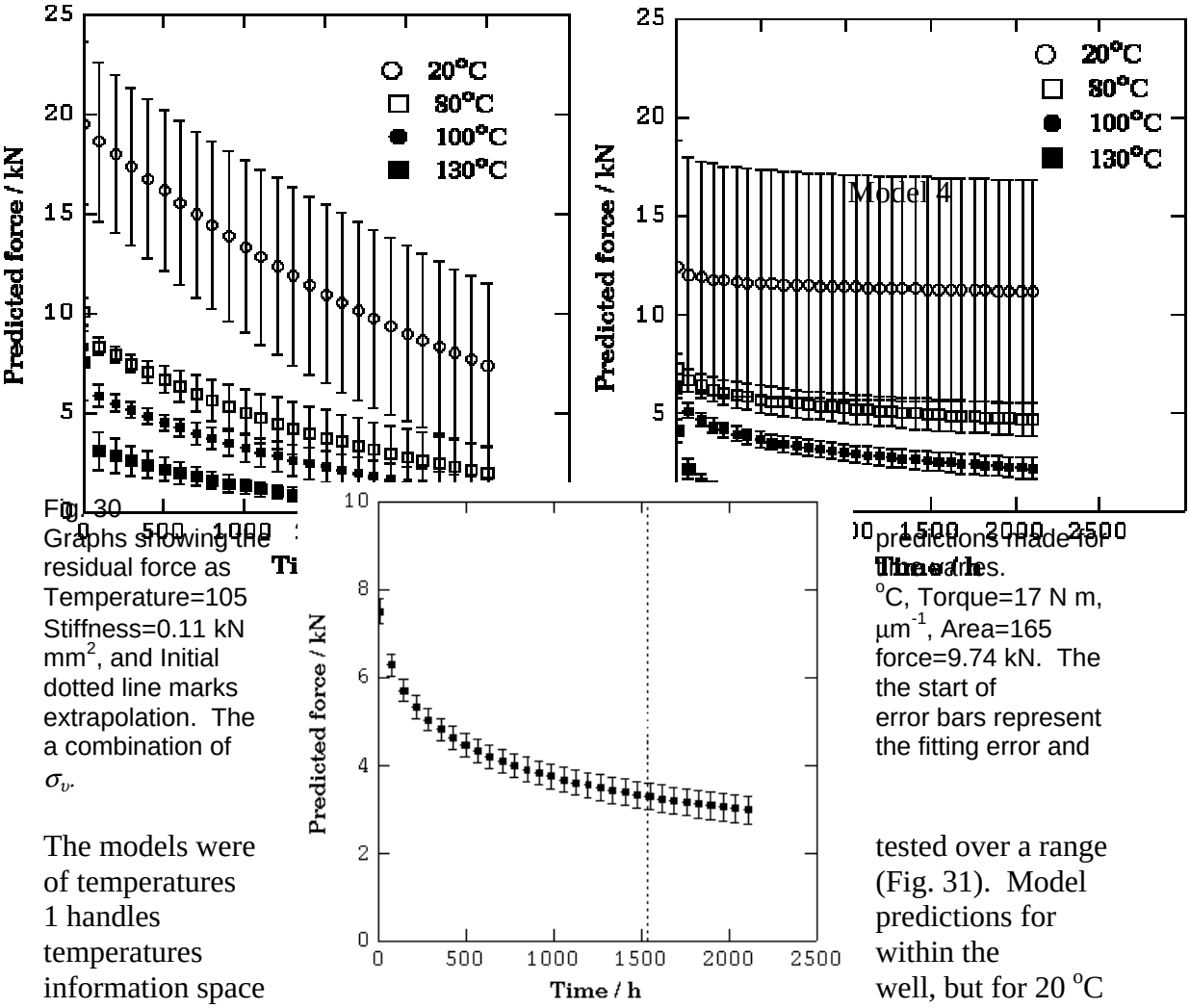

Fig. 30
Graphs showing the predictions made for residual force as Temperature=105 °C, Torque=17 N m, Stiffness=0.11 kN μm^{-1}, Area=165 mm^2, and Initial force=9.74 kN. The dotted line marks the start of extrapolation. The error bars represent a combination of the fitting error and σ_v.

The models were tested over a range of temperatures (Fig. 31). Model 1 handles predictions for temperatures within the information space well, but for 20 ^oC the prediction is less good. At room temperature there should be much less diffusion of magnesium than at 100 ^oC and so there should not be as much stress relaxation as at 100 ^oC. The predictions made by both models agree in that it is possible to draw a line through the prediction made by Model 1, which lies within the prediction of Model 3. Model 3 predicts an almost horizontal line for 20^oC, but with large error bars. This shows that the model is uncertain because it has no data at temperatures of 20^oC but the prediction follows standard diffusion behaviour. For 130^oC, the Model 3 prediction shows that no force will be present in the bolt after 650 hours; this time period is short enough to be consistent with the accepted maximum service temperature of 125^oC [32].

Model 3

Fig. 31
Predictions for residual force as time varies and at different temperatures using (from left to right) Models 1 and 2. Torque=17 N m, Stiffness=0.11 kN μm^{-1}, Area=165 mm^2 and Initial force=9.74 kN. The error bars represent a combination of the fitting error and σ_v. Both graphs show the prediction made by the model at zero time rather than the initial force.

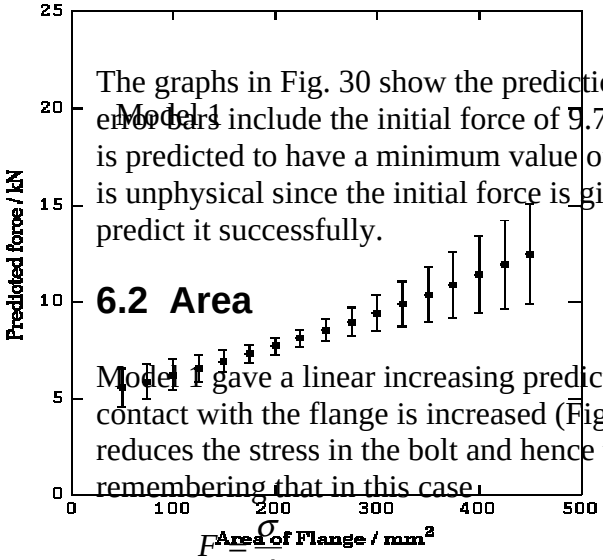

Model 1

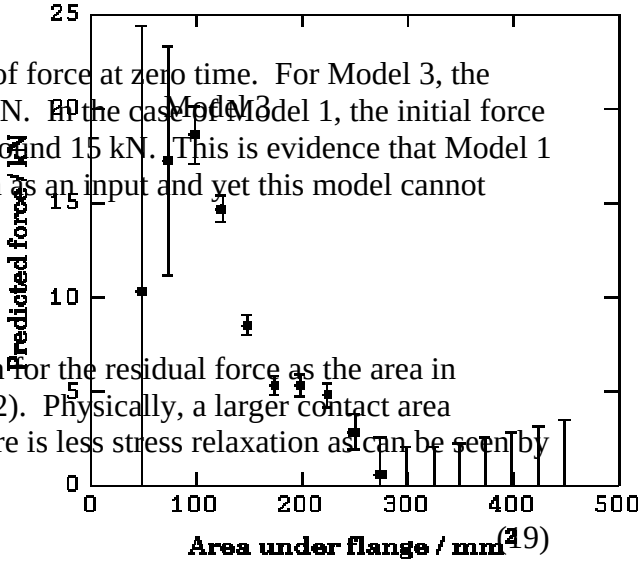

Model 3

The graphs in Fig. 30 show the prediction of force at zero time. For Model 3, the error bars include the initial force of 9.74 kN. In the case of Model 1, the initial force is predicted to have a minimum value of around 15 kN. This is evidence that Model 1 is unphysical since the initial force is given as an input and yet this model cannot predict it successfully.

6.2 Area

Model 1 gave a linear increasing prediction for the residual force as the area in contact with the flange is increased (Fig. 32). Physically, a larger contact area reduces the stress in the bolt and hence there is less stress relaxation as can be seen by remembering that in this case

$$F = \sigma A \quad (19)$$

where F = force, σ = stress and A = area the stress is applied to[6] and so for a given stress, increasing area decreases the residual force. The prediction made by Model 1 is therefore wrong. The same trend can be seen in the prediction made by Model 4.

Fig. 32

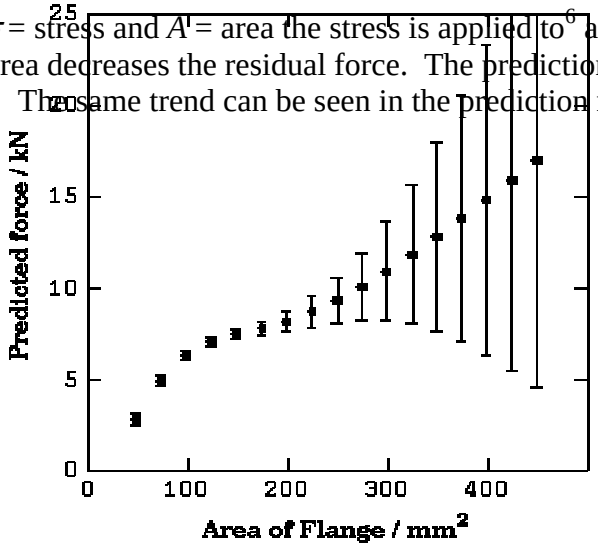

Model 4

[6] *A* here is the same as the *A* in the compliance calculations used in Model 4.

Graphs showing the predictions made for force as area varies. Temperature=105 ^{o}C, Torque=17 N m, Stiffness=0.11 kN μm^{-1}, Initial force=9.74 kN and Time=6 h. The error bars represent a combination of the fitting error and σ_v. The prediction made by Model 3 is based on varying the $\ln\sigma$ input.

The prediction made by Model 3 is the only one to agree with the physical trend that increasing area should decrease the force. The strange form of the error bars in the prediction could be a result of area not being an individual input to Model 3. The effect of area is incorporated in the $\ln\sigma$ input, so increasing area reduces the initial force. As shown below, initial force is proportional to the residual force and so the strange shape of the prediction is actually correct. For the first portion, where the residual force is shown to increase, the effect of reducing the initial force is not very significant. However, when the area increases to about 100 mm^2, the initial force effect becomes dominant and the overall trend shows a decrease in clamping force.

6.3 Initial Force

The initial force, F_{start}, is given by

$$F_{start} = \frac{\sigma_{start}}{A} \tag{21}$$

where it is assumed that $\sigma \propto \sigma_{start}$

$$\therefore F \propto F_{start} . \tag{22}$$

The predictions should be of the form of a linear increasing function (Fig. 33).

Model 1 makes such a prediction, as does Model 4, albeit with some variation in the error bars. Model 3 predicts a curve with a turning point at a starting force of 17 kN, however the subsequent error bars are large and could contain a curve that continued to increase beyond this. The predictions of Model 3 for area and starting force are related mathematically in a *y = f(x)* and *y = constant - f(x)* relationship, ie one curve is a scaled reflection in the line *y = const*ant of the other. This is confirmation of the effect of the combined $\ln\sigma$ input discussed above.

The prediction made by Model 1 is fundamentally wrong, despite having the correct shape. The predicted force for zero initial force is about 3 kN, which is simply impossible. For low initial forces the other models have large error bars which include zero.

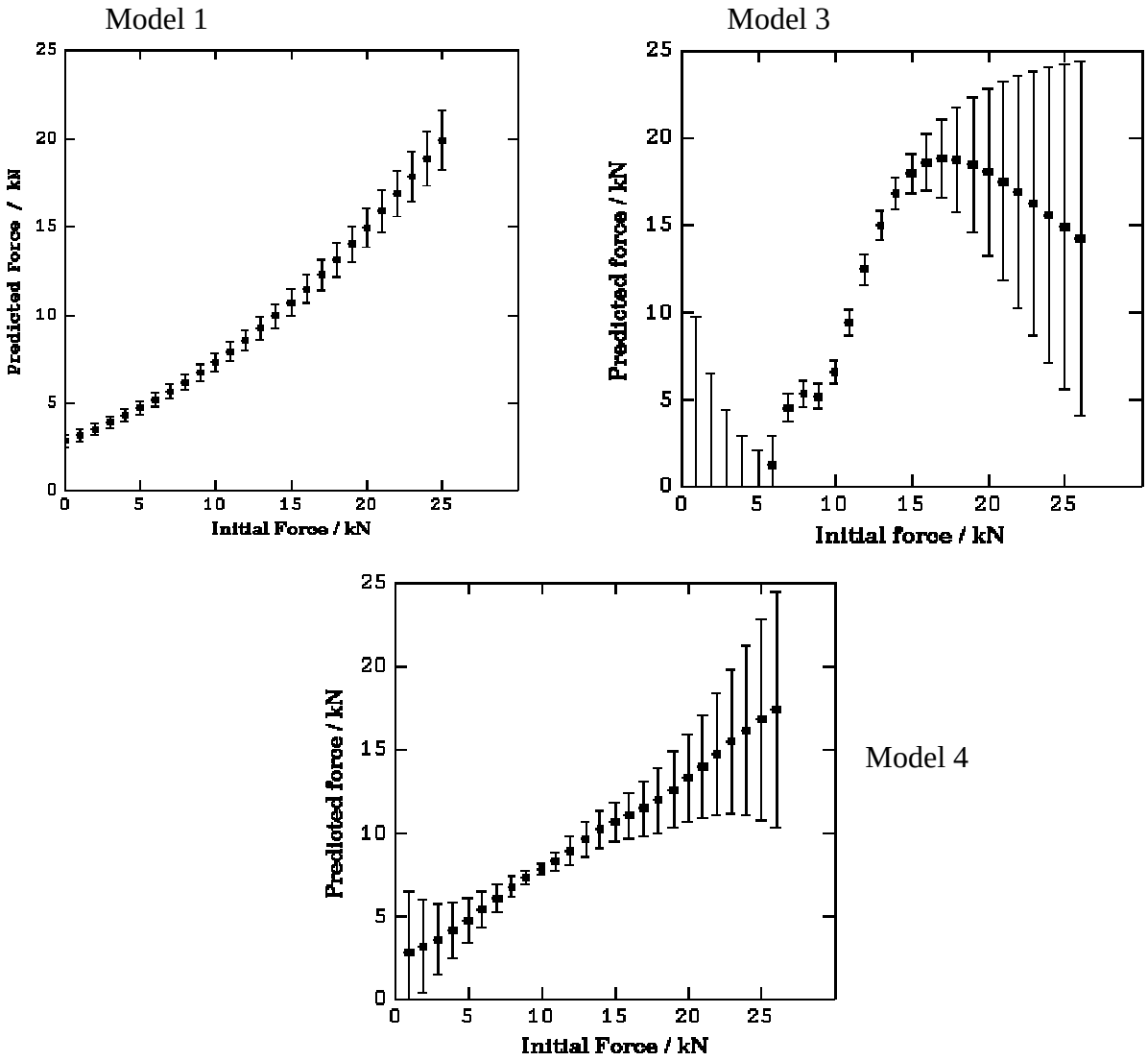

Fig. 33
Graphs showing the predictions made for force as initial force varies. Temperature=105 ^{o}C, Torque=17 N m, Stiffness=0.11 kN μm^{-1}, Area=165 mm^{2} and Time=6 h. The error bars represent a combination of the fitting error and σ_v. The prediction made by Model 3 is based on varying the lnσ input.

6.4 Stiffness

Model 3 does not have stiffness as an input and so it cannot make predictions for the behaviour of stiffness, although the effect of stiffness is included implicitly in the stress. Both Models 1 and 4 predict a decreasing trend for the residual force as the stiffness is increased (Fig. 34).

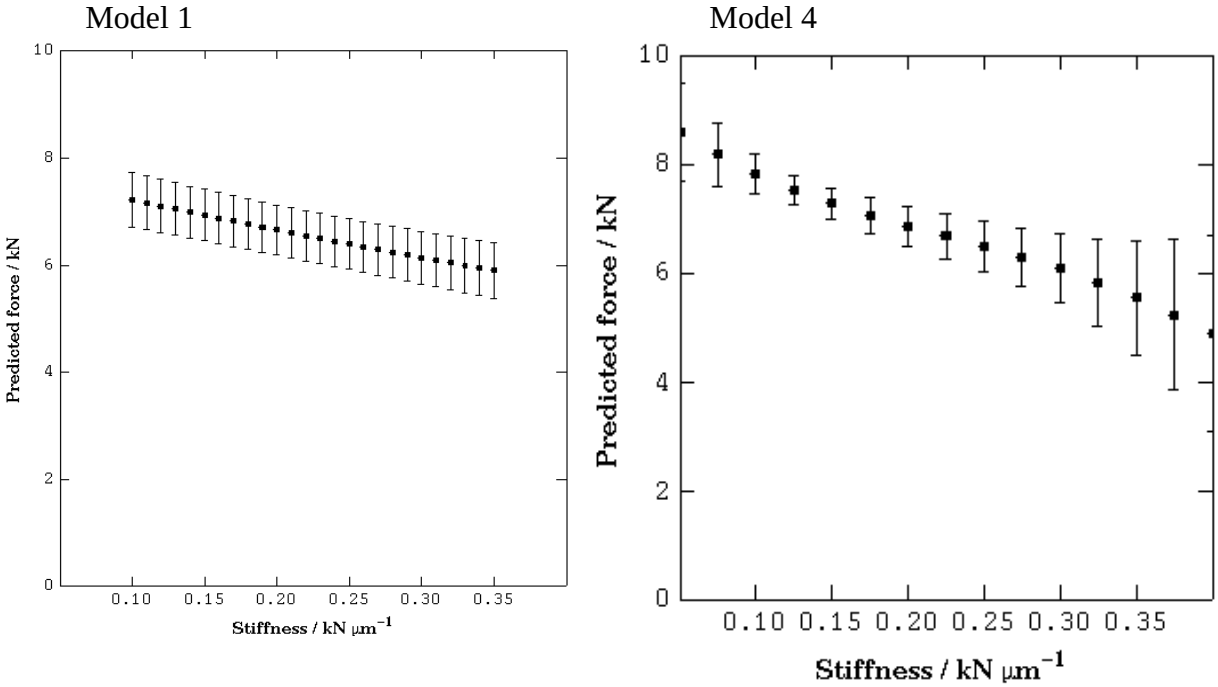

Fig. 34
Graphs showing the predictions made for force as stiffness varies. Temperature=105 ^{o}C, Torque=17 N m, Area=165 mm^{2}, Initial force=9.74 kN and Time=6 h. The error bars represent a combination of the fitting error and σ_{υ}. There is no prediction for Model 3 because it does not include stiffness as an input.

Comparing the stress-strain curves for high stiffness and low stiffness materials shows that relaxing to a given strain will result in different amounts of stress relaxation; the high stiffness material will have a much larger amount of stress relaxation than the low stiffness material (Fig. 35). Therefore using a material with a small Young's modulus for the bolt will reduce the stress relaxation when compared with a bolt that has a high Young's modulus. This effect could also be achieved by using a washer of a low Young's modulus material.

The calculations not only predict the physical trend, but the models agree very well with each other and there is scope within the error bars for both models to be making the same prediction.

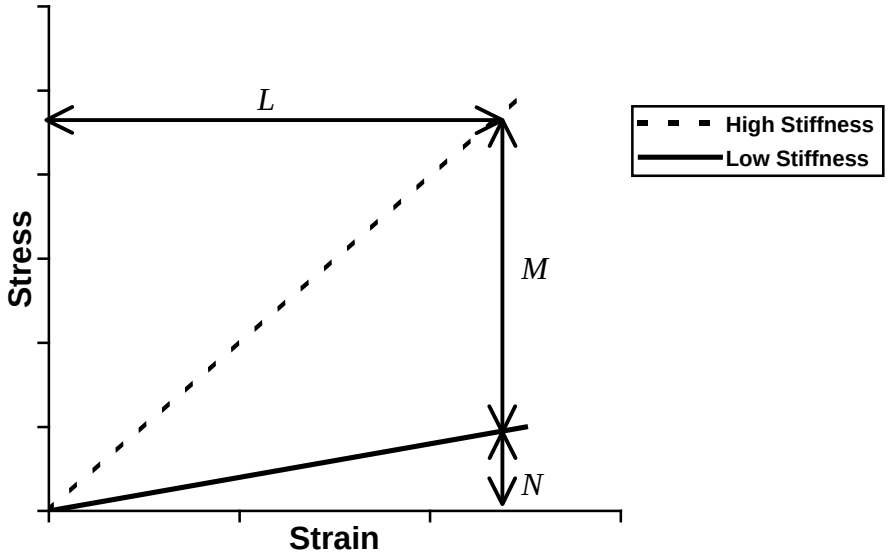

Fig. 35
Sketch showing the effect of stiffness on strain and stress for a given material. Reducing the strain by *L* causes the high stiffness material to relax by stress *M+N* and the low stiffness material to relax by stress *N*.

6.5 Temperature

As temperature increases, the amount of diffusion increases exponentially causing the residual force to decrease (1). All three models predict this trend (Fig. 36).

At first glance it seems that the prediction made by Model 1 is not physical. If the error bars were to permit a linear trend then the shape of the graph could be excused as being due to uncertainty. It is not possible to draw a straight line through the error bars of Model 1's prediction. Therefore, if the prediction is physical, either the plot has a minimum or the curve asymptotically approaches the temperature axis. A minimum is completely unphysical, since differentiating the creep equation (1) with respect to temperature gives

$$\frac{d\dot{\varepsilon}}{dT} = -\frac{Q}{RT^2} A\sigma^n e^{-Q/RT} \tag{23}$$

which has no turning points. However, there would not be any turning points if the curve were asymptotically approaching the axis. The error bars show a 65% confidence interval (1σ). A confidence interval of 95% (2σ) would permit a linear trend, without either a turning point or asymptotic behaviour. Therefore it is not clear whether the temperature dependence of Model 1 is a physical prediction.

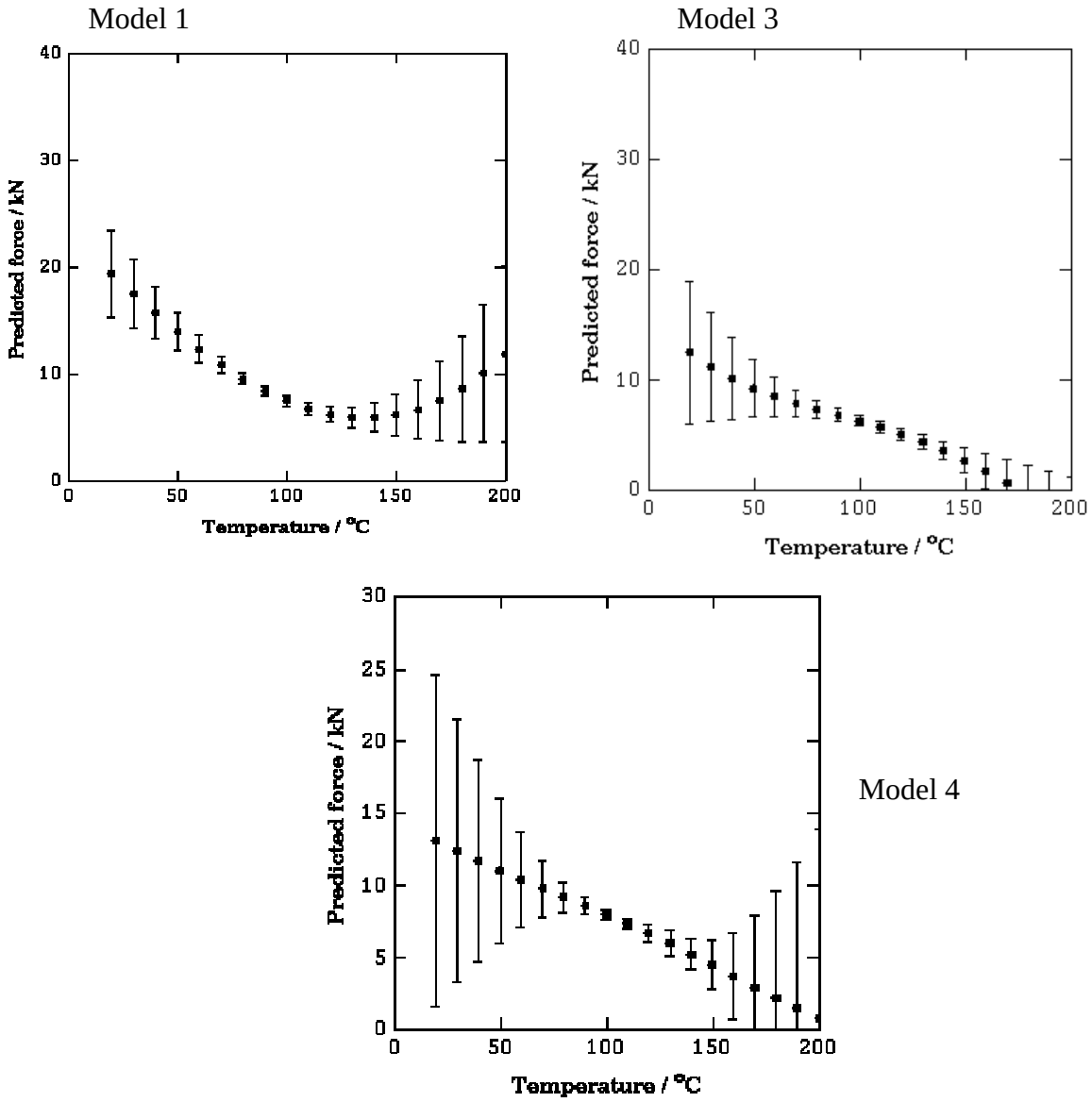

Fig. 36
Graphs showing the predictions made for force as temperature varies. Torque=17 N m, Area=165 mm^2, Stiffness=0.11 kN μm^{-1},Initial force=9.74 kN and Time=6 h. The error bars represent a combination of the fitting error and σ_v. The prediction for Model 3 is shown in °C (rather than in K) to aid comparison.

7 Application of Model

In 1997 Chen *et al*. conducted experiments in bolt load retention on a variety of magnesium alloys [38]. The models detailed above were used to attempt to reproduce these results. Before this work could begin, it was necessary to convert the results of Chen *et al*. (1997) from the dimensionless $F(t)/F_{start}$ format to $F(t)$. Various data points were taken and mathematical software was used to make a regression analysis of the curves, which were then plotted (Fig. 37).

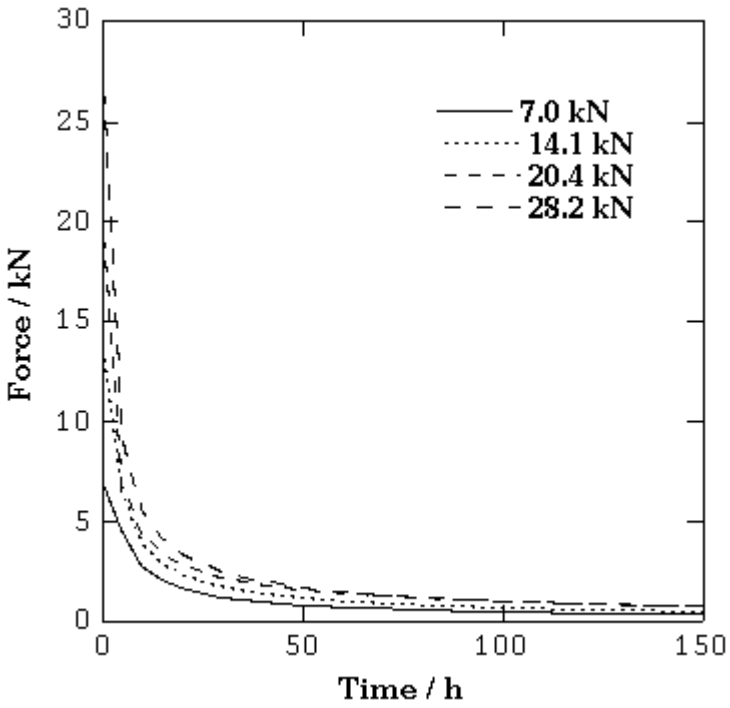

Fig. 37
Reproduction of Chen *et al*. (1997) results, un-normalised.

The predictions of the various models are shown, with error bars that include the fitting error and σ_v; Chen *et al*. did not publish their experimental errors (Fig. 38). These plots are on the same scale as Fig. 37.

The models all predict curves of the same shape as the results that Chen *et al*. obtained. The error bars are large because the temperature of Chen *et al*.'s experiment, 175°C, was much greater than the highest temperature, 130°C, in the original dataset. The high temperature also explains why the models all predict total relaxation by about 100 hours, independent of the initial force. Where the predictions appear to be missing, they were negative, implying total relaxation.

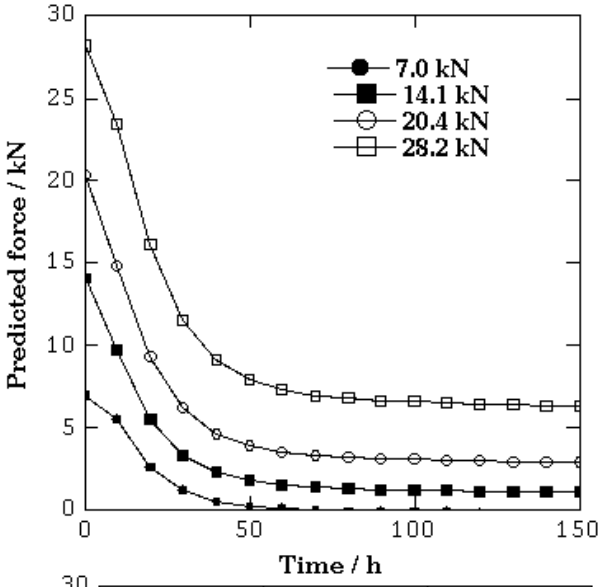
Predicted force / kN
Time / h
7.0 kN
14.1 kN
20.4 kN
28.2 kN

Fi
Pr
wi
cc

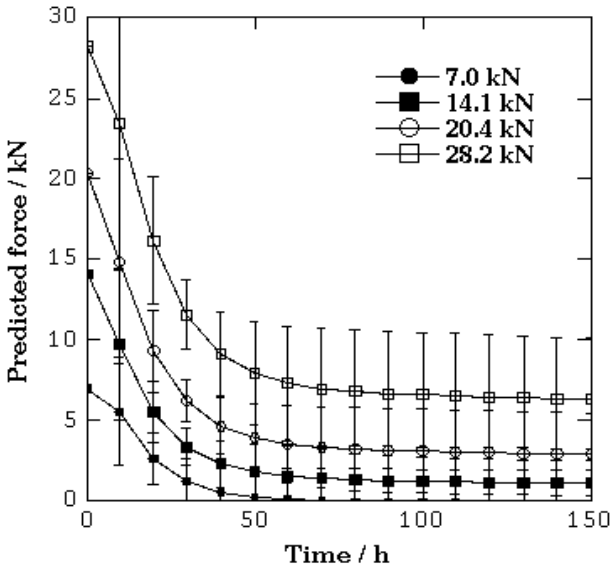
Predicted force / kN
Time / h
7.0 kN
14.1 kN
20.4 kN
28.2 kN

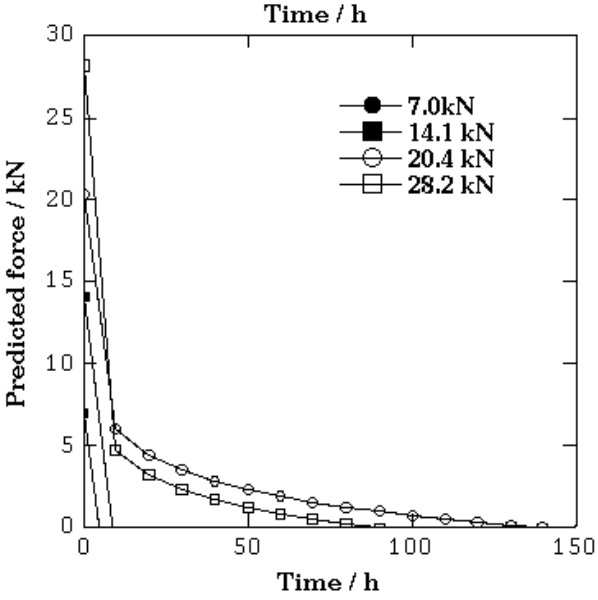
Predicted force / kN
Time / h
7.0kN
14.1 kN
20.4 kN
28.2 kN

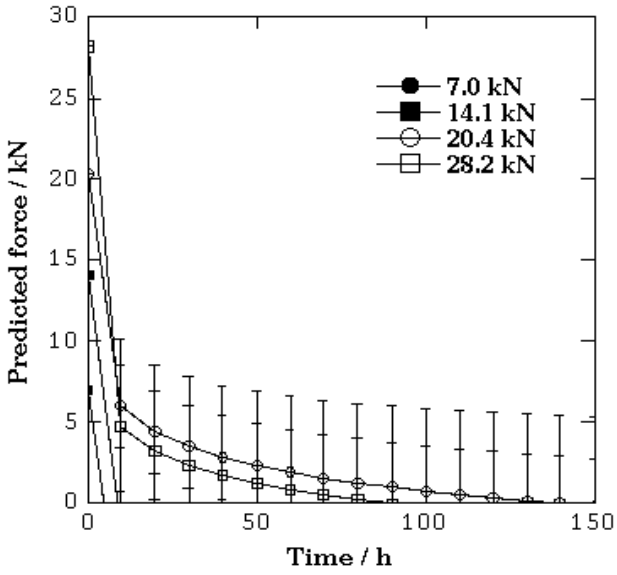
Predicted force / kN
Time / h
7.0 kN
14.1 kN
20.4 kN
28.2 kN

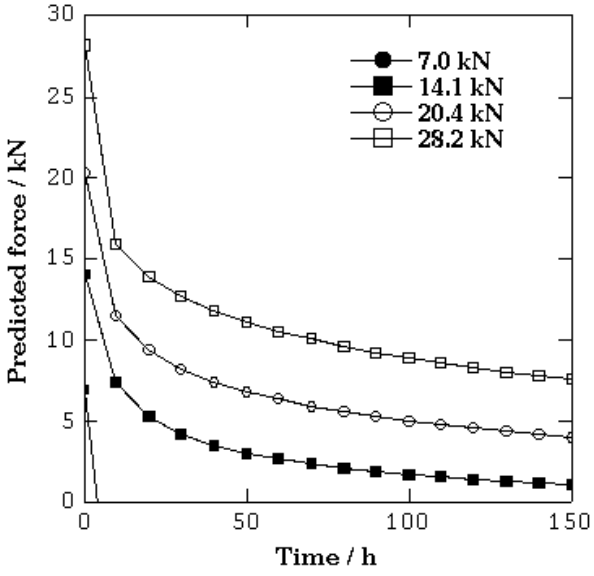
Predicted force / kN
Time / h
7.0 kN
14.1 kN
20.4 kN
28.2 kN

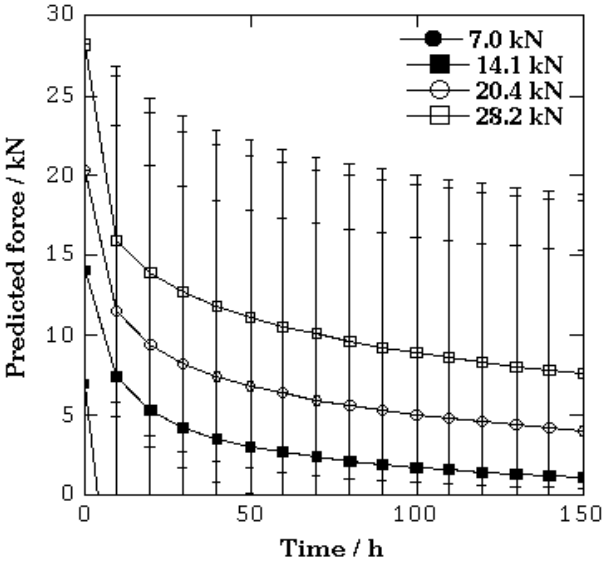
Predicted force / kN
Time / h
7.0 kN
14.1 kN
20.4 kN
28.2 kN

A glance at Fig. 28 shows that only Model 3 predicts almost complete relaxation of stress after 100 hours. The other models show residual stresses of appreciable magnitude continuing even after 150 hours. This is especially true when the initial force was large. The asymptotic behaviour seen in the predictions made by Model 1 and Model 4 is not desirable.

The prediction made by Model 3 shows very rapid relaxation for small loads. To try to reproduce this effect more closely, Model 5 was created using the same database as Model 3, and the same inputs, but with Chen *et al.*'s data included.

The level of perceived noise (0.11286) in Model 5 was similar to that of Model 3 (0.1243). The additional data increased the complexity of the model; five submodels were used in the committee (Fig. 39).

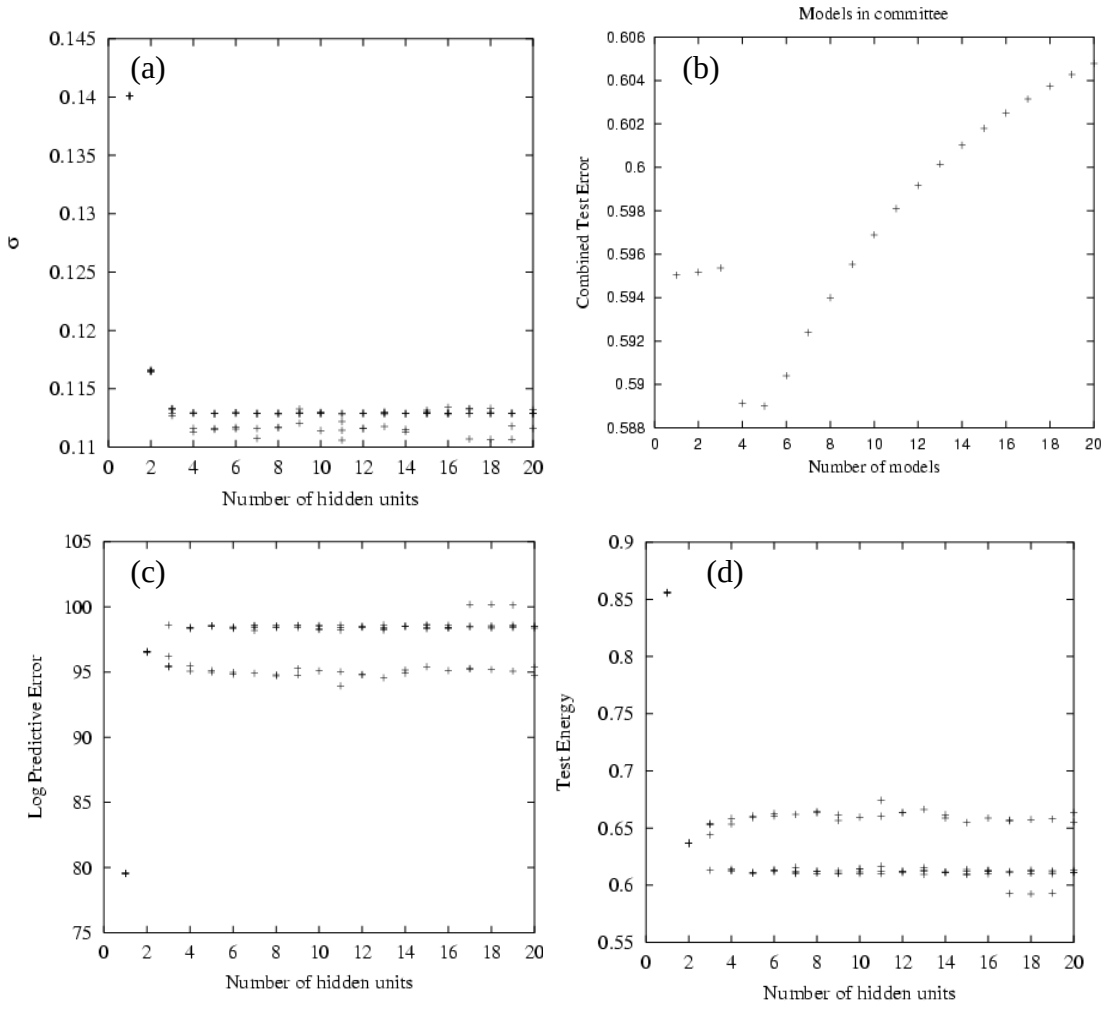

Fig. 39
The graphs used to determine the size of the committee of submodels for Model 5: (a) perceived noise (σ) vs number of hidden units; (b) CTE vs number of models; (c) LPE vs number of hidden units; (d) TE vs number of hidden units.

The graph of predicted force against actual force is shown in Fig. 40. This graph shows almost exactly the same distribution of points as the equivalent graph for Model 3. This similarity is expected and shows that if the previous predictions for Model 3 were repeated with Model 5, they would be very similar.

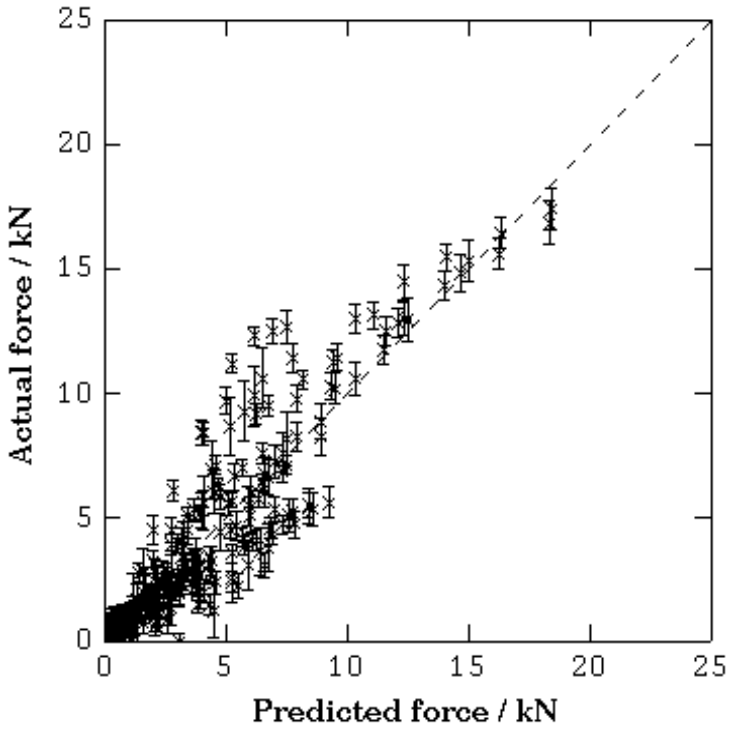

Fig. 40
Graph of actual, or experimentally measured, force versus force predicted by Model 5. The dashed line shows the perfect correlation of predicted = actual. This is a committee prediction using the entire dataset. The error bars represent a combination of the fitting error and σ_v.

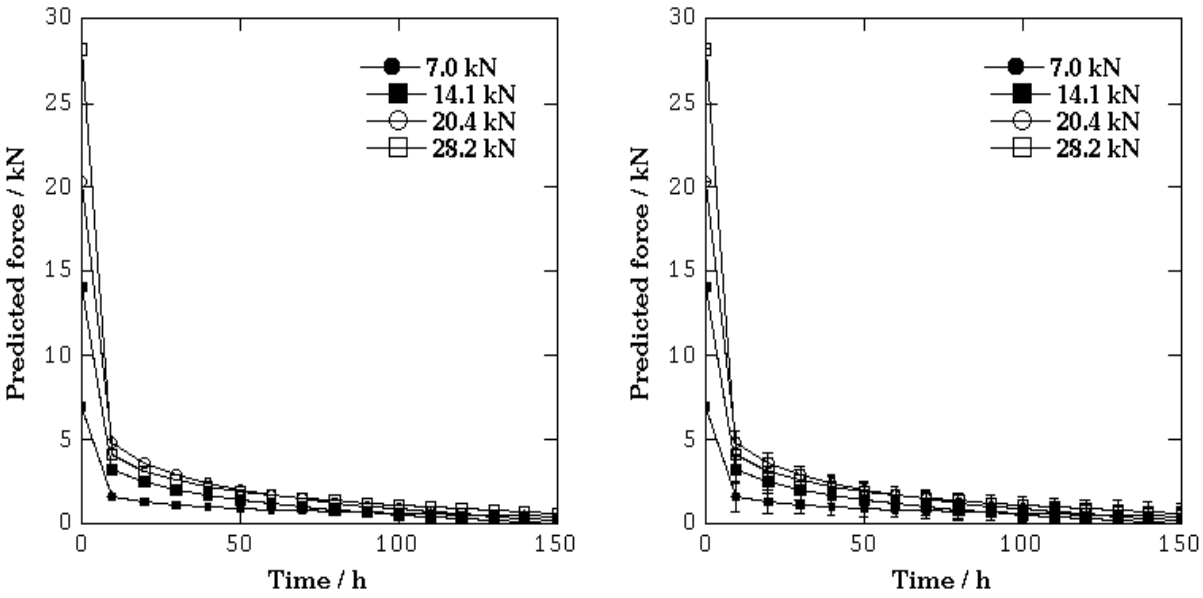

Fig. 41
Model 5's predictions of Chen et al's results, without and with error bars. The error bars represent a combination of the fitting error and σ_v.

The predictions made by Model 5 are shown in Fig. 41. The relaxation behaviour is closer to the published results than Fig. 38. The improvement in this prediction illustrates the improvements that are possible with only a small amount of additional data and underlines the advantages of a physically based model.

8 Determination of the activation energy for stress relaxation of magnesium

The equation for steady-state creep

$$\dot{\varepsilon} = A\sigma_s^n e^{-Q/\ RT} \tag{1}$$

can be applied to the data and from this a value of Q obtained [50]. A plot of $\ln\dot{\varepsilon}$ versus $1/T$ should be a straight line with gradient $-Q/RT$, for a regime of constant stress [50]. The models do not calculate the strain rate, or even the strain but the strain rate can be estimated as:

$$\dot{\varepsilon} = \frac{F_1 - F_2}{AE(t_2 - t_1)} \tag{24}$$

where F_i = the residual force at time t_i, A = area and E = Young's modulus of the bolt.

The linear approximation for the relationship between ε and $\dot{\varepsilon}$ is justified because the strain intervals are small. Blum *et al.* (1991) include an $\dot{\varepsilon}$ - ε for AZ91D at 135 ^{o}C which shows that for strains below 0.075, the relationship is approximately linear [14]. This further justifies the above approximation.

Model 3 was used for this calculation since it correctly produces physical trends. The graphs are shown in figures 42 – 45. The results given in Table 8 are for the first 10 hours of stress relaxation. Results beyond this point gave decreasing values for Q, with little difference between the value of Q for different starting stresses by 100 hours.

Table 8
Results for Q. The stress was applied to a bolt with area 165 mm^2 at a temperatures from 75-150 ^{o}C. The regression (best fit), minimum and maximum values of Q are given. The minimum and maximum values were found from the lines of maximum and minimum gradient that could be drawn within the error bars shown in Figs. 40 - 43. The error bars define the 65% confidence interval.

Stress (MPa)	Best fit value of Q (kJ mol^{-1})	Minimum value of Q (kJ mol^{-1})	Maximum value of Q (kJ mol^{-1})
50	55	12	71
75	122	25	175
100	104	-100	291
125	55	-166	299

These results show some agreement with the published value of 135 kJ mol^{-1} [27]. Other authors have published results of 130 kJ mol^{-1} [27] and 146.9 kJ mol^{-1} under 100 MPa [21]. The variation in these results are consistent with the parts of information space that are known. The stresses found in the database are between 36 MPa and 86MPa. The amount of uncertainty in Q increases as the stress increases.

Although these results show large intervals within which Q could be, all of these intervals contain the published value. For a stress of 75MPa, the model calculates Q to be 122 kJ mol $^{-1}$, which is 90% of the published value. Given that the perceived noise in Model 3 is 12%, this shows that Model 3 is accurately reproducing the physics of stress relaxation.

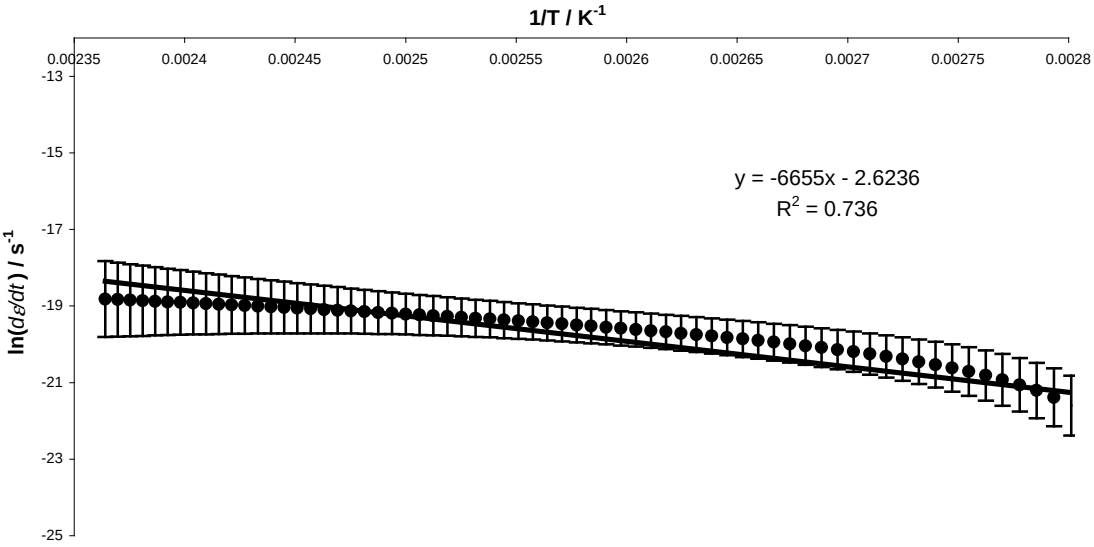

Fig. 42
Graph used to determine Q for a stress of 50 MPa. The error bars represent the fitting error for the predicted force. A line of best fit has been plotted; its equation is given in the form $y = mx+c$. The R^2 value is a measure of how well the line is fitted to the data. R^2 is defined by

$$R^2 = 1 - \frac{\sum_i \left(Y_i - \overline{Y_i}\right)^2}{\left(\sum_i Y_i^2\right) - \frac{1}{n}\left(\sum_i Y_i\right)^2}$$ for n points Y_i distant from the regression line, mean $\overline{Y_i}$.

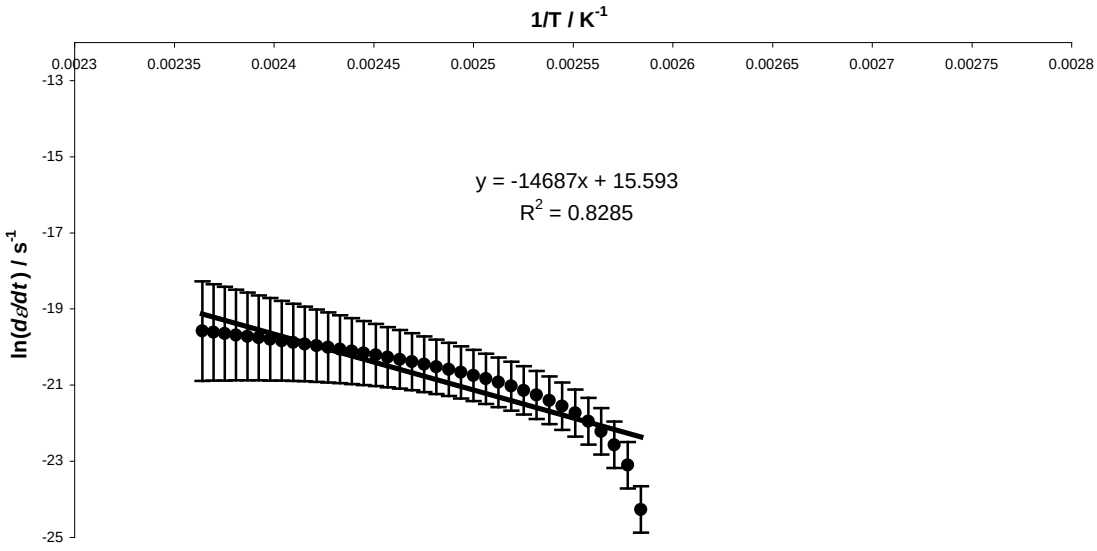

Fig. 43
Graph used to determine Q for a stress of 75 MPa.

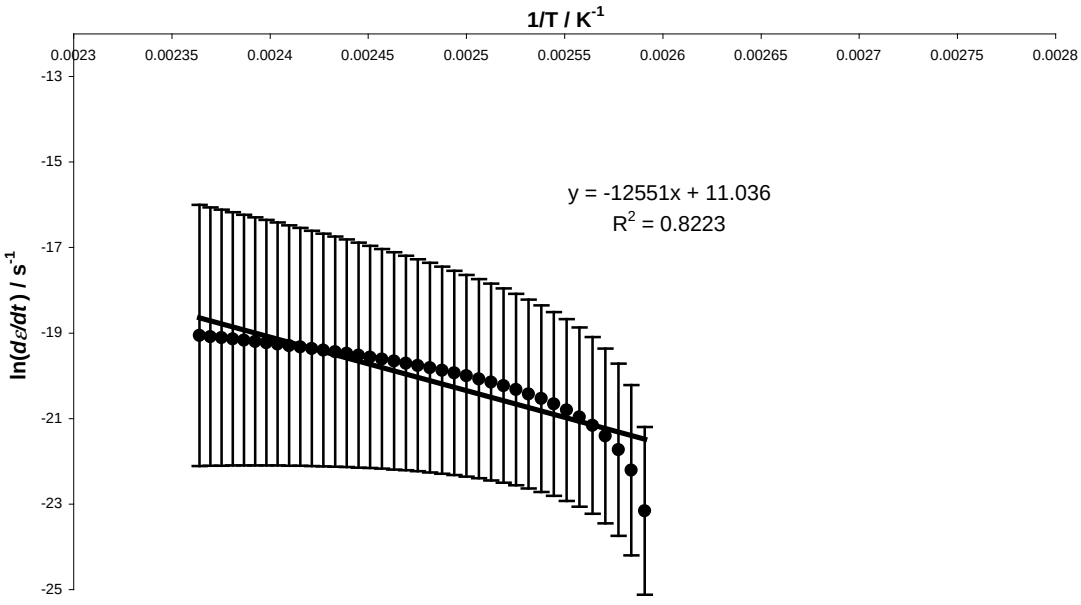

Fig. 44
Graph used to determine Q for a stress of 100 MPa.

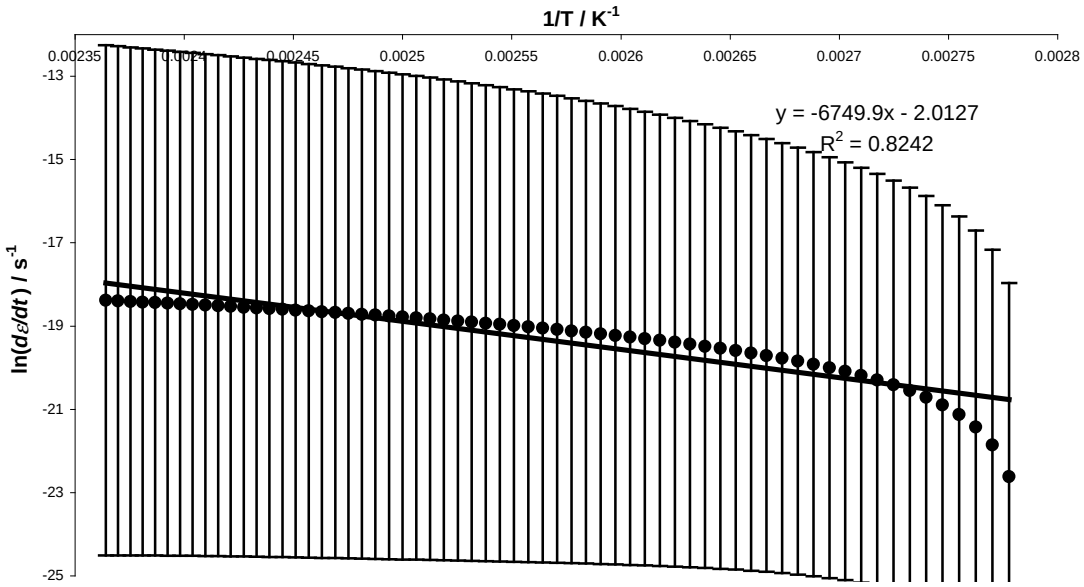

Fig. 45
Graph used to determine Q for a stress of 125 MPa.

9. Conclusion

In this section I shall discuss the predictions and limitations of each model. Then I will compare the neural network method used here to the empirical methods employed by others. Next I shall consider the problem of stress relaxation set out in the introduction and consider the advances made by this work. Finally, I will consider extensions to this work.

9.1 The Models

9.1.1 Model 1

This model was created using only the data in the database; there were no physical inputs. It was instrumental in the project in that the physics it suggested were followed up in the later models. However, this model itself was not physical.

Model 1's predictions for any input other than time do not show physical trends. The trend for time itself is not completely physical, as shown by the reproduction of Chen *et al.*'s results. The long term trend for time, accelerated by the high temperature used in Chen *et al'*s experiments, shows that a settled residual force is reached, that can be as much as one quarter of the initial force. If this were true, then all that would be necessary to use AZ91D components would be careful preloading at high temperature in the factory. In high temperature conditions, total relaxation should occur in a finite time, therefore Model 1 is unphysical.

9.1.2 Model 2

Model 2 included all the original data inputs used in model and combined these with the diffusion inputs used in Model 3. The result could have been very good, especially given the low level of noise. This was not the case. The predictions produced by Model 2 showed trends that were completely the wrong shape, even in the known areas of information space. The model was so obviously unphysical from such an early stage that very little work was completed using it.

The catastrophe of Model 2 illustrates the dangers of adding inputs, particularly inputs that duplicate information. The software used has an automatic relevance determination facility, which meant that the significance of some of the combined inputs was very small when compared with the individual inputs. However, this did not prevent the introduction of bias. Model 2 is an example of a poor attempt to construct a neural network.

9.1.3 Model 3

Model 3 included the diffusion inputs alone, thus avoiding the pitfalls encountered when running Model 2. The predictions produced by this model were all physical. It was the only model to predict, for example, complete relaxation rather than residual force decreasing to a constant value.

Model 3 illustrates nicely the improvement in performance possible when physical insight is used to construct a model, rather than just data. The contrast with Model 1 is particularly interesting. The level of perceived noise is similar, despite Model 3 being constructed from a smaller database than Model 1. The predictions for time for

these two models are at first glance similar but with larger error bars on Model 1's prediction. Closer inspection reveals that apart from the initial force, the prediction made by Model 1 is almost linear, whereas Model 3's prediction shows a curve. The curve is what we physically expect, although, it is contained by the error bars of Model 1.

The predictions made by Model 3 are all physical. The predictions for area and initial force, which are linked together in the $\ln\sigma$ input, are physical, but include the effect of the inputs being combined. Model 3 is by far the most useful model of the four and correctly reproduces the physics of stress relaxation.

Model 3 also confirms that stress relaxation can be approximated by steady-state creep, if it could not then this model would not have been successful. The correct calculation of the activation energy for self-diffusion in magnesium at a stress of 75 MPa confirms that self-diffusion is an important mechanism in stress relaxation. With more data, a more certain value could be obtained. Also, the calculation of the activation energy confirms that this model does reproduce the correct physics.

The success of Model 3, and its extension (Model 5), when applied to Chen *et al.*'s published results is further evidence that a physical model makes better predictions than an empirically based one.

Model 3 is the best model produced. The success of Model 3 and the failure of the other models underlines the superiority of neural networks with physical inputs over those without.

9.1.4 Model 4

Model 4 is based on the compliance approach, which postulates that the residual force is directly proportional to the fifth root of the time and inversely proportional to area. The predictions produced are all non-physical. In particular, the residual force does not appear to experience total relaxation as time progresses, but instead approaches a constant value, which is greater than the error bars on both Model 1 and Model 3 allow. The predictions made for stiffness and temperature appear to be physical, but the other predictions are not.

It is difficult to determine whether Model 4 offers an improvement over Model 1. It is certain that this technique is limited in application and that the approximation for the compliance is wrong. The link between stiffness and compliance does not seem to produced a physical model. The significance graphs of all the models show that the stiffness is the least important input. Therefore it is not surprising that a model which concentrates on compliance (stiffness) is not very successful.

9.2 Neural networks versus empirical methods

Neural networks are increasingly being used as an alternative to traditional empirical methods to solve complicated problems. Traditional regression methods have given scientists insights into mechanisms, such as the regression based derivation of the steady-state creep equation (1). The method of fitting a function to a set of data is limited to datasets that can be plotted on a graph. This makes regression a "two-dimensional" approach. For problems that are more complicated, many more dimensions than two are often present. The graphs of showing the significances of the inputs to the models, show that at least three inputs are required to describe stress relaxation, $\ln\sigma$, $1/T$ and $\ln t$. However, $\ln\sigma$ is a compound input containing information about the applied force, the area it is applied to and information about the stiffness of the bolt, making stress relaxation a five dimensional problem. It would be surprising if an empirical model were capable of reproducing this complicated problem accurately.

As shown in section 3, there are a variety of empirical methods in use. Some of these, [26, 33, 34, 35] are partially based on the steady-state creep equation, others on the compliance method [36, 37, 38]. The success of Model 3 shows that inputs derived from the steady-state creep equation can be used to model stress relaxation successfully. The advantage Model 3 has over empirical methods is that it can make predictions outside of its dataset. These predictions contain a measure of uncertainty, but the amount of it is shown in the predictions. This is not possible with a model based only on a line of best fit. The failure of Model 4 to make physical predictions beyond its dataset, clearly illustrates the restrictions of an empirical model. This model consistently predicted a residual force that was significantly larger than the other models. This failure shows how dangerous an empirical method can be; a car designed using the predictions made by this model would be unsafe.

The technique of using neural networks is often described as being a "black box". I believe this is partly because the method is defined in terms of frightening equations but it also illustrates the Achilles heel of the neural network method: it is very difficult, if not impossible, to discover ***precisely*** what is happening inside the network. The technique can produce answers, but cannot explain why. To use a neural network requires a good physical understanding of the problem and careful consideration of the likelihood of the results. Empirical methods are often used for this. The form of the relationship between variables cannot be found directly from a neural network, but an empirical method can determine it. Both techniques should be used together when tackling a problem, there should not be "competition" between the methods but "cooperation".

9.3 The future for magnesium alloys in car engines

The demands facing automobile manufacturers for lighter, cleaner and safer cars are unlikely to diminish. Today's generation are more aware of environmental issues than any before, and they are also conscious of value for money. Per kilogram, it is cheaper to process magnesium than aluminium. The price of pure magnesium, which dominates the cost of all magnesium alloys, is likely to decrease as demand increases [9]. The supply of magnesium is at present limited only by the small number of extraction facilities. There are many benefits of magnesium over aluminium with the added bonus of not sacrificing strength.

Magnesium is not the "dream material" it seems to be. As well as the benefits there is the problem of stress relaxation. At present, designs eliminate this small difficulty by using magnesium only for room temperature applications, body parts etc. If magnesium is to be used at higher temperatures, it is necessary to be able to model the progress of stress relaxation.

Predictions have been made by the models to show the effect of varying all the defining variables on the residual force. The engineer is most concerned with the combined effects of temperature and time. The predictions of Model 3 show that the force in the bolt will be less than half the starting force by 250 hours and that at 130 ^{o}C total relaxation occurs in 500 hours. These predictions reveal the severity of stress relaxation as a design issue. The large amount of stress relaxation shown to occur in such a short time period, relative to the lifetime of the vehicle, suggests that engineers would do better with a different material.

Despite this bleak outlook, it is important to remember that the alternative alloys available are too expensive for use in cars. There are alternatives in development, but it is unlikely that they will be tested and refined to an extent suitable for use in car engines for some time. The future of magnesium alloys in car engines is likely to rest with one of these developmental alloys. Meanwhile, the technology to use alloys, such as AZ91D, is available for manufacturers to exploit. The advantages of magnesium alloys justify the amount of research interest, it is just not clear that much progress can be made with AZ91D.

The predictions made by Model 3 suggest that using AZ91D at temperatures around 100 ^{o}C is not a good design choice. Coupled with the results in [23], the predictions show that at these temperatures AZ91D is severely limited. The obvious solution of welding, rather than bolting the components together, is at present not viable. Not only are magnesium alloys unsuited to welding, but welding joins makes replacing parts much more difficult. As the predictions based on stiffness show, reducing the Young's modulus of the bolt will reduce the amount of relaxation. Lack of data has prevented the prediction of residual force for other materials, despite the models being material independent. It is certain that to use AZ91D the bolts would have to be carefully chosen. One possibility would be to use aluminium bolts and another to add a washer of memory metal alloy.

The problem of stress relaxation will always be present for magnesium alloys, even when the new generation of (relatively) creep resistant, affordable alloys is available.

This work shows that the best method for analysing stress relaxation is a neural network.

9.4 Extensions

These models are material dependent as far as the material the bolt is made from is concerned. To extend this to alloy independence would require a database of stress relaxation data including other alloys. Then a much more powerful model would be produced which would enable engineers to compare the new alloys about to emerge onto the market.

Many of the predictions made contain reasonably large error bars, indicating that the model is very uncertain about this region of information space. This problem could be reduced and a better model produced, simply by adding more data to the database. This is illustrated by the improvement in Model 5 over Model 3, where the only difference was that Model 5 had more data.

Some of the inputs to the model, such as area, could almost be described as discrete, with as few as 3 different values. In the case of area, the predictions show that increasing the area decreased the stress relaxation. If data were available concerning different areas of contact it would be possible to investigate the affect of bolt geometry on relaxation, following the work of Pettersen *et al*. (2001), which shows that changing bolt geometry has implications for the stiffness [16]. Reducing the area reduces the stiffness of the bolt, which has been shown to reduce the relaxation. This extension combined with using a low Young's modulus material for the bolt may make AZ91D a practical material for engine applications.

10 References

[1] http://www.aspireuk.net/autoimports
(2001)

[2] http://www.nadaguides.com
(2001)

[3] http://europa.eu.int/comm/environment/enlarg/handbook/air.pdf
(2001)

[4] http://www.ford.com/servlet/ecmcs/ford/index
(2001)

[5] http://www.thenewsteel.com
(2001)

[6] K.H. Matucha: *Materials science and technology: a comprehensive treatment, Volume 8: Structure and properties of nonferrous alloys*
Weinheim (1996), Series Editors: R.W. Cahn, P. Haasen & E.J. Kramer

[7] http://www.hydromagnesium.com
(2001)

[8] http://www.magnesium.norada.com
(2001)

[9] P.D. Caton: *Magnesium – an old material with new applications*
Materials and Design **12 (6)** (1991) 309-316

[10] http://www.austmg.com
(2001)

[11] http://minerals.usgs.gov/minerals/pubs/commodity/aluminium/050301.pdf
(2001)

[12] http://minerals.usgs.gov/minerals/pubs/commodity/magnesium/400301.pdf
(2001)

[13] S. Paetke: *A study of the microstructure and stress relaxation of spring steels*
Thesis held at Department of Materials Science and Metallurgy, University of Cambridge (1980)

[14] W. Blum, P. Weidinger, B. Watzinger, R. Sedlacek, R. Rosch & H.-G. Haldenwanger: *Time dependent deformation of the magnesium alloys AS21 and AZ91*
Zeitschrift für Metallkunde **88 (8)** (1997) 636-641

[15] M. Regev, E. Aghion, S. Berger, M. Bamberger & A. Rosen: *Dislocation analysis of crept AZ91D ingot castings*
Materials Science and Engineering **A 257** (1998) 349-352

[16] K. Pettersen & s. Fairchild: *Stress relaxation in bolted joints of die cast magnesium components*
SAE Technical Paper Series, Preliminary Results
Society of Automotive Engineers

[17] E.F. Emley: *Principles of magnesium technology*
Pergamon Press (1966)

[18] A. Luo & T. Shinoda: *A new magnesium alloy for automotive powertrain applications*
SAE Technical Paper Series, **980086**
Society of Automotive Engineers (1998)

[19] W.E. Mercer II: *Magnesium die cast alloys for elevated temperature applications*
SAE Technical Paper Series, **900788**
Society of Automotive Engineers (1990)

[20] B.R. Powell, V. Rezhets, M.P. Balough, R.A. Waldo: *The relationship between microstructure and creep behaviour in AE42 magnesium die casting alloy*
Magnesium Technology 2001, Editor: J.N. Hryn
The Minerals, Metals & Materials Society (2001)

[21] S. Spigarelli: *Creep of a thixoformed and heat treated AZ91 Mg-Al-Zn alloy*
Scripta Materialia **42** (2000) 397-402

[22] L.L. Shreir, R.A. Jarman & G.T. Burstein: *Corrosion 1: Metal / environment reactions*
Butterworth-Heinemann (1994)

[23] M. Regev, O. Botstein, M. Bamberger & A. Rosen: *Continuous vs interrupted creep in AZ91D magnesium alloy*
Materials Science & Engineering A **A302** (2001) 51-55

[24] http://www.hghouston.com/glossary
(2001)

[25] I.J. Polymear: *Light alloys – metallurgy of the light metals*
Edward Arnold (1981)

[26] W.K. Miller: *Creep of die cast AZ91 magnesium at room temperature and low stress*
Metallurgical Transactions A **22A** (1991) 873-877

[27] K.Y. Sohn, J.A. Yurko, F.C. Chen, J.W. Jones & J.E. Allison: *Creep and bolt-load retention behaviour of die-cast magnesium alloys*
Automotive Alloys II, Editor: S.K. Das
The Materials, Metals & Minerals Society (1998)

[28] M.O. Pekguleryuz: *Development of creep resistant magnesium diecasting alloys – an overview*
http://www.magnesium.norada.com/img/develop.pdf
(2001)

[29] A.A. Luo & B.R. Powell: *Tensile and compressive creep of magnesium-aluminium-calcium based alloys*
Magnesium Technology 2001, Editor: J.N. Hryn
The Minerals, Metals & Materials Society (2001)

[30] B.R. Powell, A.A. Luo, V. Rezhets, J.J. Bommarito, B.L. Tiwari: *Development of creep-resistant magnesium alloys for powertrain applications: Part 1 of 2*
SAE Technical Paper Series, **2001-01-0422**
Society of Automotive Engineers (2001)

[31] M.F. Ashby & D.R.H. Jones: *Engineering materials: an introduction to their properties and applications*
Pergamon Press (1982)

[32] H.J. Frost & M.F. Ashby: *Deformation-mechanism maps for metals and alloys*
Pergamon Press (1982)

[33] F.V. Ellis & S. Tordonato: *Calculation of stress relaxation properties of type 422 stainless steel*
Journal of Pressure Vessel Technology **122** (2000) 66-71

[34] M. Tendo, K. Yamada & Y. Shimura: *Stress relaxation behaviour at high-tension bolted connections of stainless-steel plates*
Journal of Engineering Materials and Technology **123** (2001) 198-202

[35] T.K. Aune & T.J. Ruden: *High temperature properties of magnesium die casting alloys*
SAE Technical Paper Series, **920070**
Society of Automotive Engineers (1992)

[36] J. Bolton: *Design considerations for high temperature bolting*
Performance of bolting materials in high temperature plant applications
Editor: A. Strang
Institute of Materials (1995)

[37] J. Yang & T.J. DeWolf: *Mathematical model for relaxation in high-strength bolted connections*

Journal of Structural Engineering **August** (1999) 803-809

[38] F.C. Chen, J.W. Jones, T.A. McGinn, J.E. Kearns, A.J. Nielsen & J.E. Allison: *Bolt-load retention and creep of die-cast magnesium alloys*
SAE Technical Paper Series, **920070**
Society of Automotive Engineers (1992)

[39] A. Luo & T. Shinoda: *A new magnesium alloy for automotive powertrain applications*
SAE Technical Paper Series, **980086**
Society of Automotive Engineers (1998)

[40] J.C.M. Li: *Dislocation dynamics in deformation and recovery*
Canadian Journal of Physics **45** (1967) 493-509

[41] H.K.D.H. Bhadeshia: *Neural networks in materials science*
ISIJ International **39 (10)** (1999) 966-979

[42] M. Evans: *Method for improving parametric creep rupture life of 2.25Cr-1Mo steel using artificial neural networks*
Materials Science and Technology **15** (1999) 647-658

[43] J. Tenner, D.A. Linkens, P.F. Morris & T.J. Bailey: *Prediction of mechanical properties in steel heat treatment process using neural networks*
Ironmaking and Steelmaking **28 (1)** (2001) 15-22

[44] D.J.C. MacKay: *Probable neural networks and plausible predictions – a review of practical Bayesian methods for supervised neural networks*
http://wol.ra.phy.cam.ac.uk/mackay/BayesNets.html
(2001)

[45] S.H. Lalam, H.K.D.H. Bhadeshia & D.J.C. MacKay: *Estimation of mechanical properties of ferritic steel welds*
Science and Technology of Welding and Joining **5 (3)** (2000) 135-147

[46] D.J.C. MacKay: *Bayesian non-linear modelling with neural networks*
http://wol.ra.phy.cam.ac.uk/mackay/BayesNets.html
(1995)

[47] D.J.C. MacKay: *Bigback neural network simulator*
http://wol.ra.phys.cam.ac.uk/mackay/SourceC.html
(2001)

[48] D.L. Albright & T.K. Aune: *Stress relaxation behaviour of die casting alloys*
SAE Technical Paper Series, **910412**
Society of Automotive Engineers (1991)

[49] K.Y. Sohn, J.A. Yurko, J.W. Jones, J.E. Kearns & J.E. Allison: *Bolt-load retention behaviours of die-cast AZ91D and AE42 magnesium*
SAE Technical Paper Series, **980090**
Society of Automotive Engineers (1998)

[50] R.W. Evans & B. Wiltshire: *Creep of metals and alloys*
The Institute of Metals (1985)

[51] J.R. Taylor: *An introduction to error analysis; the study of uncertainties in physical measurements*
University Science Books (1997)

11 Appendices

Appendix A – Nomenclature

Inputs to the models are emboldened. The list is divided into three: the notation associated with steady-state creep; the notation used to describe the models; and the notation used in the theory of neural networks.

$\dot{\varepsilon}$ strain rate s^{-1}
σ initial stress MPa
Q activation energy for self-diffusion in magnesium kJ mol^{-1}
T **temperature ^{o}C (sometimes K)**
R molar gas constant 8.314472 J K^{-1} mol^{-1}
12 **A** ***constant (only in the context of steady-state creep)***
n power law exponent

B, C constants
m, δ power law exponents
ε strain (no units)
t **time h**
S **stiffness kN μm^{-1}**
C **compliance μm kN^{-1}**
α thermal expansion coefficient K^{-1}
l length
A **stressed area**
E Young's modulus (usually of the bolt) GPa
$\boldsymbol{F_{start}}$ **initial force kN**
F residual force **(model output)** kN

x input vector
y output vector
w weight vector
t target vector
θ bias
σ_v perceived noise
σ_w significance of input

11.2 Appendix B – Calculation of Stiffness

11.2.1 Derivation of stiffness addition rule

By definition, strain $\varepsilon = \frac{\sigma}{E}$ where σ = stress and E = Young's modulus.

Also, extension $\Delta l = L\varepsilon$ where L = total length.

$\therefore \Delta l = \frac{\sigma}{E} L$ and if $\sigma = \frac{F}{A}$ where F = applied force and A = area then

$\Delta l = \frac{FL}{AE}$

By dimensional analysis[7], stiffness $S = \frac{F}{\Delta l} = \frac{AE}{L}$.

For two materials in series e.g. a bolt with a steel shaft and an aluminium head, the strains in each material are given by $\varepsilon_1 = \frac{\sigma}{E_1}$ and $\varepsilon_2 = \frac{\sigma}{E_2}$ for a constant stress.

Total extension $\Delta l = \Delta l_1 + \Delta l_2$ where Δl_1 = extension in material 1 and Δl_2 = extension in material 2.

$$\therefore \Delta l = \varepsilon_1 L + \varepsilon_2 L = \frac{\sigma}{E_1} L_1 + \frac{\sigma}{E_2} L_2 = \frac{F}{A}\left(\frac{L_1}{E_1} + \frac{L_2}{E_2}\right)$$

The combined stiffness $S_C = \frac{F}{\Delta l} = \frac{A}{\left(\frac{L_1}{E_1} + \frac{L_2}{E_2}\right)}$

Considering $\frac{1}{S_C} = \frac{L_1}{AE_1} + \frac{L_2}{AE_2} = \frac{1}{S_1} + \frac{1}{S_2}$ gives the stiffness addition rule, which can be extended to add any number of stiffnesses together.

11.2.2 Calculating the stiffness of a bolt

To calculate the stiffness of a bolt, it is divided into head, shank, thread and nut and these individual stiffnesses are summed using the rule just derived.

$$\frac{1}{S_C} = \frac{1}{S_{head}} + \frac{1}{S_{shank}} + \frac{1}{S_{thread}} + \frac{1}{S_{nut}}$$

The shank component has an extra term relating to the stiffness of the unthreaded length of the shank. Experiments have shown that a more precise estimate of stiffness can be gained if the constituent stiffnesses are weighted before summing.

$\therefore \frac{1}{S_C} = \frac{1.1d}{EA_X} + \frac{L_1}{EA_1} + \frac{1.6d}{EA_X} + \frac{0.6d}{EA_X} + \frac{0.5d}{EA_X}$ where E = Young's modulus of the bolt material and the remaining quantities are the dimensions shown in Fig. 46.

[7] The units of stiffness are kN μm^{-1}.

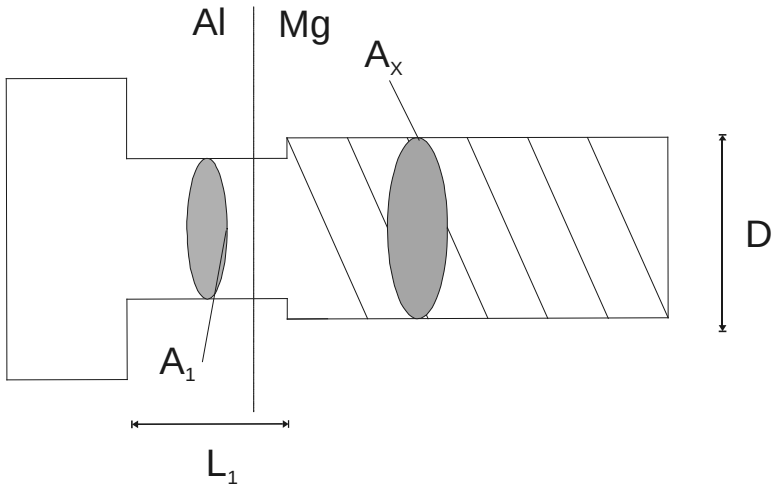

Fig. 46
Diagram of bolt labelling dimensions used to calculate stiffness. D on the diagram is identical to d in the discussion.

$$\therefore \frac{1}{S_C} = \frac{3.8d}{EA_X} + \frac{L_1}{EA_1}$$

This is only true if the bolt is completely engaged, i.e. the bolt is screwed in as far as possible.

Typically, the calculated stiffness is 10-15% higher than the experimentally measured stiffness.

11.3 Appendix C – Calculation of Experimental Error

11.3.1 Definitions and rules[8]

Any measured quantity, x or y, has an associated uncertainty δx, δy respectively. The result of a measurement is given as $x \pm \delta x$. The fractional uncertainty of x is defined as $\frac{\delta x}{|x|}$.

The "rules" used in the calculation below:

1. If $q = xy$ then $\frac{\delta q}{|q|} = \frac{\delta x}{|x|} + \frac{\delta y}{|y|}$.
2. If $q = Bx$ where B is a number then $\delta q = |B|\delta x$
3. If $q = q(x,\ldots\ldots,y)$ and if $\{\delta x,.....\delta y\}$ are independent random variables then
$$\delta q = \sqrt{\left(\frac{\partial q}{\partial x}\delta x\right)^2 + ... + \left(\frac{\partial q}{\partial y}\delta y\right)^2}$$
4. If errors are independent random variables then to combine them, add in quadrature i.e. $\delta q = \sqrt{\delta x^2 + \delta y^2}$

11.3.2 Calculation of Experimental Error

The following calculation is for an M8 bolt. The following values were used in the calculation[9]:

$A = 149\times10^{-6}$; $d = 8\times10^{-3}$; $L_1 = 20\times10^{-3}$; $A_X = 36.6\times10^{-6}$; $A_1 = 32.3\times10^{-6}$;
$E = 210\times10^{9}$; $e(0) = 24\times10^{-6}$; $F = 21.5\times10^{3}$; $t = 6$; $T = 75$

The measurements have the following uncertainties:

- Temperature: $T \pm 3$ °C
- Dimensions: $L \pm 0.2$ mm, excepting $L_1 \pm 0.5$ mm
- Elongation: $e \pm 5$ μm
- Time: $t \pm 1/60$ h

Measurement of elongation was used to determine the clamping force on the bolt at any given time. $F(t) = Se(t)$

The uncertainty for time is estimated. It has been assumed that the best estimate for experimental error will be given by $\frac{\delta q}{|q|}$ where $q \to q(T, A, S, F, t)$.

Using (4), the experimental error $\frac{\delta q}{|q|} = \sqrt{\frac{\delta T}{|T|}^2 + \frac{\delta A}{|A|}^2 + \frac{\delta S}{|S|}^2 + \frac{\delta F}{|F|}^2 + \frac{\delta t}{|t|}^2}$

From the information above, $\frac{\delta T}{|T|} = \frac{3}{75} = 0.04$

For an M8 bolt, $A = 149$ mm^2. The length measured is assumed to be the diameter, in line with engineering practice. Hence using (1) and (2),

[8] The calculation in this appendix is based on the formalism developed by J.R. Taylor [51].
[9] Torque is omitted due to it only being present in Model 1.

$$A = \frac{\pi}{4} d^2 = 149 \times 10^{-6}$$

$$\Rightarrow d = 0.01377$$

$$\therefore \frac{\delta A}{|A|} = 2\pi \frac{\delta d'}{|d|} = 2\pi \frac{0.2 \times 10^{-3}}{0.01377} = 0.09126$$

Using (3), $\delta S = \sqrt{\left(\frac{\partial S}{\partial d}\delta d\right)^2 + \left(\frac{\partial S}{\partial A_X}\delta A_X\right)^2 + \left(\frac{\partial S}{\partial L_1}\delta L_1\right)^2 + \left(\frac{\partial S}{\partial A_1}\delta A_1\right)^2}$

From the above information, $\delta d = 0.2 \times 10^{-3}$, and $\delta L_1 = 0.5 \times 10^{-3}$.
Using (1) and (2),

$$A_X = \frac{\pi}{4} d'^2 = 36.6 \times 10^{-6}$$

$$\Rightarrow d' = 6.826 \times 10^{-3}$$

$$\therefore \frac{\delta A_X}{|A_X|} = 2\pi \frac{\delta d'}{|d'|} = 2\pi \frac{0.2 \times 10^{-3}}{6.826 \times 10^{-3}} = 0.184$$

$$A_1 = \frac{\pi}{4} d''^2 = 32.2 \times 10^{-6}$$

$$\Rightarrow d'' = 6.403 \times 10^{-3}$$

$$\therefore \frac{\delta A_1}{|A_1|} = 2\pi \frac{\delta d''}{|d''|} = 2\pi \frac{0.2 \times 10^{-3}}{6.403 \times 10^{-3}} = 0.196$$

From Appendix B, $S = \frac{3.8d}{EA_X} + \frac{L_1}{EA_1}$ therefore

$$\frac{\partial S}{\partial d} = \frac{3.8}{EA_X} = \frac{3.8}{210 \times 10^9 \times 36.6 \times 10^{-6}} = 4.944 \times 10^{-7}$$

$$\frac{\partial S}{\partial A_X} = \frac{-3.8d}{EA_X^2} = \frac{-3.8 \times 8 \times 10^{-3}}{210 \times 10^9 \times \left(36.6 \times 10^{-6}\right)^2} = -1.081 \times 10^{-4}$$

$$\frac{\partial S}{\partial L_1} = \frac{1}{EA_1} = \frac{1}{210 \times 10^9 \times 32.2 \times 10^{-6}} = 1.479 \times 10^{-7}$$

$$\frac{\partial S}{\partial L_1} = \frac{-L_1}{EA_1^2} = \frac{-20 \times 10^{-3}}{210 \times 10^9 \times \left(32.2 \times 10^{-6}\right)^2} = -9.185 \times 10^{-5}$$

$$\therefore \frac{\delta S}{|S|} = \frac{9.896 \times 10^{-10}}{0.1 \times 10^9} = 9.896 \times 10^{-18} \approx 0$$

The initial force is calculated from the elongation at zero time. Using (1),
$F = Se(0)$

$$\therefore \frac{\delta F}{|F|} = \frac{\delta S}{|S|} + \frac{\delta e}{|e(0)|} \approx 0 + \frac{5 \times 10^{-6}}{24 \times 10^{-6}} = 0.208$$

From the information above, $\delta t = 0.0278$.

$$\frac{\delta q}{|q|} = \sqrt{\frac{\delta T}{|T|}^2 + \frac{\delta A}{|A|}^2 + \frac{\delta S}{|S|}^2 + \frac{\delta F}{|F|}^2 + \frac{\delta t}{|t|}^2}$$

$$\frac{\delta q}{|q|} = \sqrt{0.04^2 + 0.09126^2 + 0 + 0.208^2 + 0.0278^2}$$

$$\therefore \frac{\delta q}{|q|} = 0.232$$

The experimental error was 0.23.